Energy Conversion and Management 309 (2024) 118322

Contents lists available at ScienceDirect

Energy Conversion and Management

journal homepage: www.elsevier.com/locate/enconman

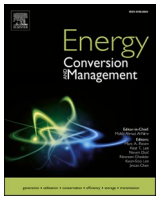

Optimal environmental and economic performance trade-offs for fifth generation district heating and cooling network topologies with waste heat recovery

Michael D. Murphy [a,b,*], Amy Allen [b,c,d], Gregor P. Henze [b,c,d], Nicholas L. Long [b,d]

[a] Department of Process, Energy and Transport Engineering, Munster Technological University, Bishopstown, Cork, Ireland
[b] Department of Civil, Environmental and Architectural Engineering, University of Colorado, Boulder, CO 80309, USA
[c] Renewable and Sustainable Energy Institute, Boulder, CO 80309, USA
[d] National Renewable Energy Laboratory, Golden, CO 80401, USA

ARTICLE INFO

Keywords:
District heating and cooling
Multi-objective optimization
Life cycle assessment
5GDHC
Network topologies
Waste heat recovery

ABSTRACT

Network topology greatly influences both the economic and environmental performance of fifth generation district heating and cooling (5GDHC) systems. In this study the optimal trade-offs between the environmental and economic performance of 5GDHC network topologies for a five-building district with waste heat recovery were explored. A life cycle assessment method was used to calculate the total life cycle CO_2 emissions (LCCO2) associated with the installation and operation of various network topologies. Twelve months of empirical data from a data center cooling system were analyzed to assess its suitability for integration into a 5GDHC system. The most suitable method for utilizing this waste heat was selected based on the ambient loop warm pipe setpoint, waste heat temperature, and district energy system configuration. A multi-objective optimization algorithm was used to select the 5GDHC network topology that provided the optimal trade-off between LCCO2 and life cycle cost (LCC). A trade-off parameter was employed to weigh the importance of each objective in the selection process. The results showed waste heat from the data center was suitable for integration into the 5GDHC system due to its availability and consistent temperature profile. When return temperatures of 25 °C or higher were available from the liquid-cooled system, direct pre-heating of the ambient loop warm pipe was found to be the most effective waste heat integration method. The selection of the network topology that provided the optimal trade-off between LCCO2 and LCC (optimal trade-off topology) was highly dependent on factors such as fuel prices, CO2 prices, electricity CO_2 emissions factors, availability of waste heat, embodied CO_2 emissions associated with network installation and network infrastructure costs. Optimal trade-off topologies produced substantial LCCO2 reductions relative to corresponding LCC increases. LCCO2 reduction to LCC increase ratios from 5.78 to 117.79 were identified with CO_2 offset costs ranging from 4.77 to 60.08 ($/t$CO_2$e).

1. Introduction

District thermal energy systems circulate a working fluid (generally steam, water, or water-mixture) through a network of pipes to connected loads, which use the system as a heat source or sink. Such systems are classified into five generations, distinguished by the nature of the working fluid and its temperature range. This work will adopt the definition proposed by [1] for fifth-generation district heating and cooling (5GDHC) systems, as ones that circulate water, or a water-and-glycol mixture, at near-ambient temperatures (generally 10—30 °C). Loads served by 5GDHC systems leverage water-source heat pumps to further temper the water to meet their heating and cooling requirements. Some 5DGHC systems are also served by centralized supply energy equipment, and in others, all primary energy equipment is distributed at the loads. 5GDHC systems allow connected buildings to serve as prosumers to draw heat from and reject heat to the network in a synergistic manner, as well as facilitating the integration of renewable thermal and waste heat sources at a lower range of temperatures than higher-temperature district heating networks from earlier generations [1]. The more moderate operating temperatures of 5GDHC systems relative to earlier generations of district heating systems also facilitate the electrification of heating equipment, which is necessary for system decarbonization [2]. Moderate water temperatures also reduce

* Corresponding author at: Department of Process, Energy and Transport Engineering, Munster Technological University, Bishopstown, Cork, Ireland.
E-mail address: michaeld.murphy@mtu.ie (M.D. Murphy).

https://doi.org/10.1016/j.enconman.2024.118322
Received 21 December 2023; Received in revised form 23 February 2024; Accepted 14 March 2024
Available online 27 April 2024
0196-8904/© 2024 The Author(s). Published by Elsevier Ltd. This is an open access article under the CC BY-NC license (http://creativecommons.org/licenses/by-nc/4.0/).

Nomenclature

Symbols

α	number of connected graphs
γ	pareto trade-off parameter
ε	heat exchanger effectiveness
η	Carnot effectiveness factor
θ	energy (J)
ρ	density (kg/m^3)
Cp	specific heat capacity (J/kg·K)
Cap	capacity (kg)
CC	CO_2 of combustion (kgCO_2e/l)
D	distance (m)
E	energy consumption (kWh)
F	fuel economy (l/km) (l/hr)
K	cost ($)
l	length (m)
m	mass (kg)
M	number of buildings
N	subset number of buildings connected
P	productivity (m^3/hr)
r	radius (m)
R	rotation rate (RPM)
T	temperature (°C)
V	volume (m^3)

Abbreviations

5GDHC	fifth generation district heating and cooling
CHP	combined heat and power
COP	coefficient of performance
DES	district energy system
DH	district heating
DHC	district heating and cooling
DHW	domestic hot water
DX	direct expansion
EC	embodied carbon
EF	emissions factor
ESIF	Energy System Integration Facility
ETS	energy transfer station
HDPE	high density polyethylene
HGV	heavy goods vehicle
HPC	high performance computing
HVAC	heating, ventilation, and air conditioning
LCC	life cycle cost
LCCO2	life cycle CO_2 emissions
LCA	life cycle assessment
LDPE	low density polyethylene
MF	multi-family
MST	minimal spanning tree
NIST	National Institute for Standards and Technology
NREL	National Renewable Energy Laboratory
OAT	outdoor air temperature
PU	polyurethane
RPM	rotations per minute
SC	space cooling
SH	space heating
TEC	total electricity consumption
TGC	total gas consumption
UPV	uniform present value
USD	United States Dollar
WLHP	water-loop heat pump

Subscripts

a	annual
B	bucket
Cloop	cool loop
Comp	compressor
Cond	condenser
e	equivalent
ele	electricity
Evap	evaporator
Exc	excavator
i	inner
Inst	installation
Invest	investment
Mat	material
max	maximum
min	minimum
o	outer
Op	operating
R	return
S	supply
top	topology
Tot	total
Tran	transport
Tren	trench
Wloop	warm loop

unwanted heat losses and gains through the distribution network and permit the use of less costly piping networks [2].

5GHDC systems share similarities with water-loop heat pump (WLHP) systems. WLHP systems connect several water source heat pumps to a building-internal loop, which allows for unoccupied zones to be completely separated from the occupied zones for fine-grained zonal control [3]. They also allow for energy balancing by utilizing heat from cooled zones to be moved to heated zones via the common water loop [4]. Essentially, a WLHP system can be viewed as a single-building realization of a district-level 5GDHC system. WLHP systems can be employed for waste heat recovery, however, the opportunities for waste heat utilization are typically limited to the waste heat sources collocated within or adjacent to the building [5], whereas in a 5GDHC system, waste heat sources can be integrated at a larger scale, and at larger distances.

Earlier generations of district thermal energy systems often used radial network topologies, in which each connected building is served by a single supply path from a central plant [6]. The ability of connected loads to offset each other's thermal energy requirements in a 5GDHC system leads to the consideration of ring or meshed network topologies, in which each load may be served by multiple supply paths. A study by [7] compared the energy performance of 5GDHC systems under ring and radial network topologies and found that ring network topologies could integrate waste heat sources more effectively. However, ring and meshed network topologies result in higher costs for piping infrastructure. Schluck et al. [8] compared the exergetic performance of two configurations of 5GDHC systems: a two-pipe system with bi-directional mass flow, and a single-pipe system with uni-directional mass flow. The authors found that the bi-directional system, with a meshed network topology, resulted in greater exergetic efficiency than the system with uni-directional mass flow.

The nature of 5GDHC systems motivates consideration of different design approaches, and optimization considerations than earlier generations of district thermal energy systems. A study by Zarin Pass et al. [9] established a metric for thermal load diversity under which a 5GDHC system in a particular configuration offered an improvement in exergetic

efficiency relative to building-level systems. The authors quantified the beneficial effects of greater thermal load diversity on the exergy performance of 5GDHC systems as this facilitates the ability of loads to offset the need for active conditioning of the loop.

Past work has also addressed network topology optimization of district thermal energy systems. A study by Mertz et al. [10] optimized network topology, as well as pipe diameter and system operating parameters, for minimum life cycle cost (LCC) in the context of a district heating (DH) system. Mertz et al. considered the selection of loads to be served as well as the network by which they were connected and considered parallel and series connections. Mertz et al. performed the analysis for several potential configurations of building locations and loads, concluding that the nature of the optimal topology was not readily generalizable. A study by Falke et al. [11] performed multi-objective optimization for a DH and electrical energy system. Falke et al. considered the selection of loads for connection to the thermal network, the design and operation of primary equipment, and selection of load-reduction measures at the building level. They excluded meshed thermal networks from consideration. They concluded that, for the conditions they analyzed, distributed combined heat and power (CHP) with auxiliary heat generation was more cost-effective than a centralized CHP system.

Best, et al. [12] approached a network topology optimization problem for a district heating and cooling (DHC) system, with the connectivity status of the considered loads taken as a boundary condition. Best et al. compared the outcome of the optimization under two different objective functions: capital cost and LCC. The authors restricted their search space to radial or ring topologies. They identified limited savings in LCC from network topology optimization under these conditions but found more significant benefits in terms of the internal rate of return. Best et al. identified the consideration of meshed network topologies as an area for further work. Given the emerging nature of 5GDHC systems, few studies to date have applied network topology optimization to this specific application. 5GDHC systems present a particularly promising application for network topology optimization, due to the ability of connected buildings to offset the heating and cooling load of the district energy system (DES).

5GDHC networks have also been identified as promising applications for low temperature waste heat recovery [13,14]. The warm ambient loops in 5GDHC networks are typically less than 30 °C, which makes them suitable for recovering waste heat from sources such as data centers and space cooling in commercial buildings [15], unlike fourth generation district heating systems which operate at greater than 50 °C [16]. The potential economic savings and environmental benefits of utilizing waste heat in 5GDHC networks have been addressed in previous studies [16,17,18]. However, no previous study has analyzed the impact of waste heat recovery on the optimal network topology of a 5GDHC system.

5GDHC networks may play an important role in decarbonizing urban heating and cooling systems [19]. The embodied and operating CO_2 emissions associated with installing and running DH systems [9] have been calculated in previous studies through detailed life cycle assessment (LCA) [20,21,22], and the CO_2 emissions associated with utilizing alternative fuel sources in DH systems have been compared and evaluated [23,24,25]. Operating CO_2 emissions have been factored into the optimization of 5GDHC systems [11,26,27]. Allen, et al. [28] and von Rhein, et al. [6] considered CO_2 prices and operating emissions within a network topology optimization problem for 5GDHC systems. Both studies found optimal network topologies for connecting buildings to a 5GDHC system. However, these studies did not consider the embodied CO_2 of the network (topology dependent) and the topologies were optimized for economic performance based on LCC only, the life cycle CO_2 (LCCO2) emissions were not considered.

The network topology of a 5GDHC system has not yet been optimized for environmental performance (minimal LCCO2) and the trade-offs that exist between the economically and environmentally optimal network topologies have not been explored. The effect waste heat recovery has on the optimal network topology selection and its decarbonization potential has not been analyzed. The impact CO_2 prices and emissions factors have on the feasibility of 5GDHC systems is unknown.

In this study, for a prototypical district with available waste heat, we address the following questions:

- Does the inclusion of embodied CO_2 through an LCA have a substantial effect on the selection of optimal 5GDHC network topologies with respect to both LCC and LCCO2?
- What is the most suitable method for integrating waste heat in this 5GDHC network application and what resulting CO_2 reductions can be achieved?
- Is the environmentally optimal network topology a fully connected network?
- What are the best trade-off network topologies that represent the Pareto optimum between the LCC and LCCO2 for this 5GDHC system?
- Can substantial LCCO2 savings be made while allowing for only relatively small increases in LCC? What are the associated costs for offsetting this CO_2?
- How does the integration of waste heat affect the selection of the optimal trade-off network topology? Does it encourage larger, better-connected networks? How does it affect the CO_2 offset cost?
- What impact do CO_2 prices and CO_2 emissions factors have on the optimal network topologies and the associated CO_2 offset costs?

To answer these questions the following tasks had to be completed: (1) Develop a model for the calculation of LCC for the network topologies applicable to the given prototypical 5GDHC system based in Golden, Colorado, USA. (2) Create an LCA model for the calculation of LCCO2 for specific 5GDHC network topologies. (3) Incorporate waste heat recovery in the network model based on empirical data from a data center in Golden, Colorado, USA. (4) Apply a multi-objective optimization algorithm for selecting the 5GDHC network topology that provides the optimal trade-off between environmental (LCCO2) and economic (LCC) performance. (5) Simulate multiple scenarios with varying operating conditions (such as CO_2 prices, electricity CO_2 emissions factors, availability of waste heat, embodied CO_2 emissions associated with network installation and network infrastructure costs). (6) Determine the optimal trade-offs for each scenario from the simulation results.

In Section 2, we present the 5GDHC system application, the LCA model, the waste heat recovery model and recorded data, the configuration of the simulated scenarios, and the modeling and optimization methods. In Section 3, the simulation results are displayed, and the optimal trade-off topologies determined. We discuss the outcomes and their applicability to future 5GDHC network topology selection. Section 4 presents the conclusions of this study by directly addressing the research questions.

2. Materials & methods

2.1. Prototypical district

A prototypical district was constructed for the purposes of evaluating 5GDHC network topologies. Building load profiles for the district were modeled using the U.S. Department of Energy's Prototype Building models, which represent the characteristics of common commercial and residential building types found in the U.S. [29]. The considered buildings were selected from the available prototype building models based on the load diversity metric proposed by Zarin Pass, et al. [9]. Three multi-family (MF) buildings, a retail building, and a hospital were selected. For the purpose of calculating pipe section lengths, the buildings were plotted on an existing block in Golden, Colorado, though they are not intended to represent the characteristics of actual buildings at that site. The layout of the prototypical district including all buildings and the DES is shown in Fig. 1. Meteorological data for Golden, Colorado

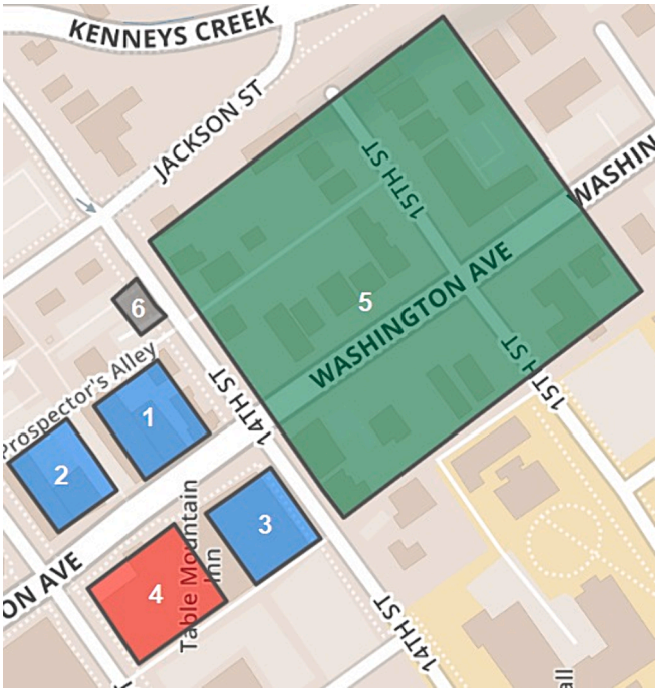

Fig. 1. Layout of the building locations in the prototypical district (courtesy of GeoJSON.io). (1) MF1, (2) MF2, (3) MF3, (4) Retail, (5) Hospital, and (6) DES.

were used in the analysis [28]. As part of this analysis, there was a need to represent the energy consumption of each prototypical building in both a connected (thermal loads served by the 5GDHC system) and independent state (thermal loads served by building-level systems). To represent the independent state, the HVAC systems present in the prototype building models remained. To represent the connected state, the building models were modified to use water-source heat pump energy transfer stations (ETS), which are served by the DES as a heat source and sink. Characteristics of the prototypical buildings, including the independent HVAC systems, are shown in Table 1, with corresponding peak and cumulative annual loads. The approach for constructing the prototypical district is explained in more detail in [28].

Fig. 2 displays the dynamic net thermal loads for the retail, multi-family and hospital buildings detailed in Table 1, along with the corresponding dry bulb outdoor air temperature (OAT). A one-week period in early October was selected as a representative week as this period was during a shoulder season which typically contains both net heating and cooling loads relative to warmer and colder OAT values.

2.2. 5GDHC networks

5GDHC networks are distinct from earlier generations of district thermal energy systems as they utilize water at more moderate, near-ambient temperatures, which facilitates the integration of a wider range of renewable and waste heat sources. Connected buildings are equipped with water-source heat pump ETSs, which use the district network as a heat source or sink. Several configurations of 5GDHC systems are used in practice. In this analysis, a 5GDHC system structured in a two-pipe configuration, permitting bi-directional mass flow was considered. The energy consumption of the system, under each possible network topology configuration, was evaluated using a model in Modelica. Modelica is an equation-based modeling language that is frequently used to represent physical systems [30]. The model used in this analysis was created by von Rhein, et al., [6] and further developed by Allen, et al., [28]. In this analysis, the modeled system's ambient loop warm pipe was controlled to a setpoint temperature of 26 °C, and the ambient loop cool pipe, 16 °C. A centralized ground-coupled water-source heat pump DES controlled the network temperature. Each connected building was served by an ETS, equipped with water-source heat pumps and circulation pumps. In the modeled ETS, a circulation pump was controlled to withdraw water from the cool or warm ambient loop pipe according to the building's required load, maintaining a 10 °C temperature differential between the two pipes. Both ambient loop pipes are connected to the DES. A schematic of this system configuration is shown in Fig. 3, the DES corresponds to the central ground-source heat pump, which is controlled to maintain the given setpoint temperatures for the warm and cool pipes. The ground source heat pump is modeled as

Table 1
Characteristics and loads of prototypical buildings.

Prototypical Building	Floor Area (m^2)	Independent HVAC System	Peak Cooling Load (kW)	Peak Heating Load (kW)	Annual Cooling Load (MWh)	Annual Heating Load (MWh)
Hospital	22,436	Variable-air volume reheat system served by water-cooled chillers and gas hot water boilers	2,972	876	1,812	1,184
Multifamily	3,120	Zone-level direct-expansion cooling and gas heating	84.9	71.9	133	57
Retail	2,295	Roof-top units with DX cooling and gas heating	88	152	64	110

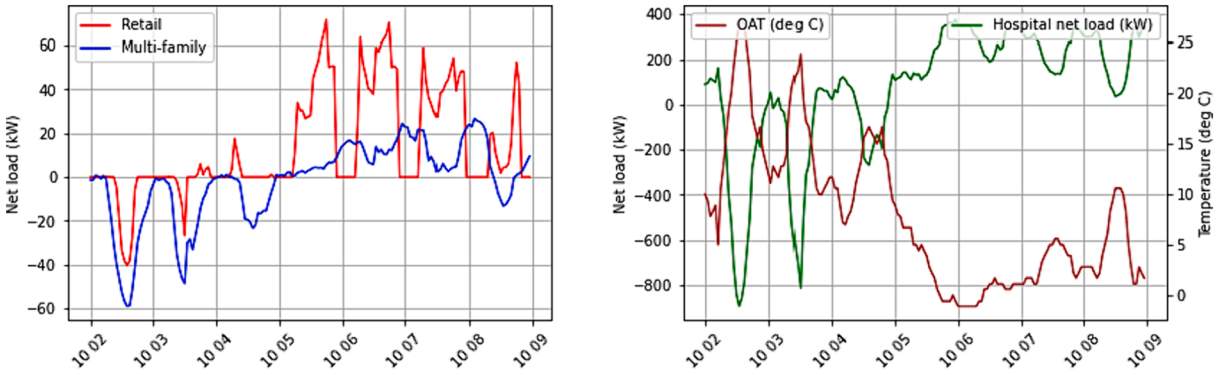

Fig. 2. Net loads (those observed by the district energy system) for each building during a week in the beginning of October, and OAT during the same period. A net heating load is shown as positive, and a net cooling load as negative.

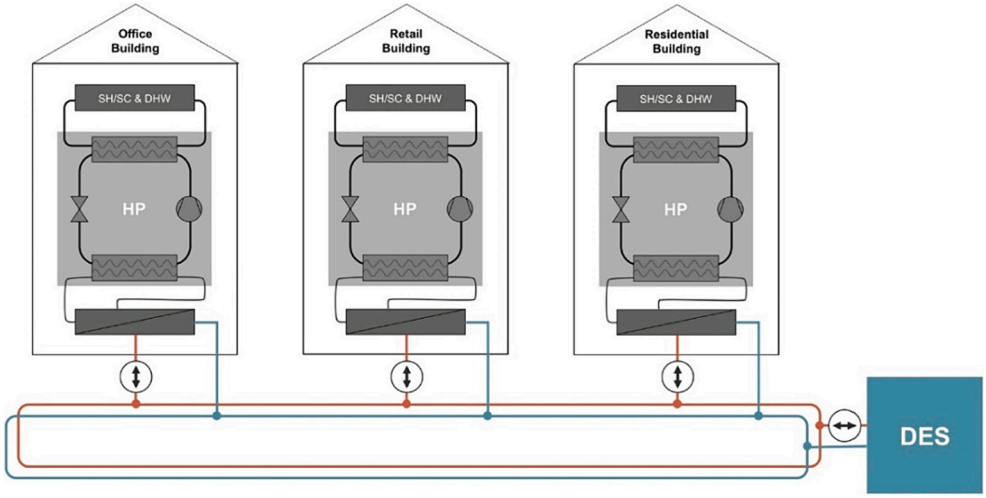

Fig. 3. Diagram of a 5GDHC network. The buildings' ETSs are connected to the warm and cool pipes of the ambient loop, which are tempered by the ground source heat pump DES. SH/SC refers to space heating and space cooling, and DHW to domestic hot water (courtesy of von Rhein et al. [6]).

operating with a mean ground temperature of 4.4 °C.

2.2.1. Network topology optimization

Several concepts from graph theory are useful in characterizing thermal networks. In the mathematical context, a graph is a set of nodes and edges, which correspond to buildings or a DES and thermal connections, respectively. The selection of the optimal subset of buildings and the selection of the optimal network by which to connect them can be considered separately. Connected graphs are of interest in the context of district thermal energy systems, with respect to the connected thermal loads. A connected graph is one in which there exists at least one path between each pair of nodes. In the case of spanning tree graphs, all nodes are still connected, but there exists only one path between each pair of nodes, therefore, in the case of a 5GDHC network, the minimal number of pipe sections is used to connect the selected buildings. A minimal spanning tree (MST) is the spanning tree graph with the minimal total length, in the case of a 5GDHC network, the minimal network length that connects the selected buildings. The MST is of interest because it connects a given set of buildings with, in this context, the least infrastructure cost associated with piping and trenching. A complete graph corresponds to the scenario in which all possible paths between nodes are present, in the case of a 5GDHC network, this results in a fully connected network. An unconnected graph is one in which one or more nodes are not connected to other nodes. In this study, if a building is not selected for connection to the network, the thermal loads are met by the building's independent HVAC system (Table 1). The optimal subset of buildings to connect to a 5GDHC network within a given district and the topology employed to connect the buildings is dependent on network investment costs, operating costs, CO_2 prices and the buildings' thermal load profiles. When substantial diversity exists between the buildings' load profiles, better-connected networks with more pipe sections directly connecting buildings (moving towards a complete graph), may reduce energy consumption. i.e. if one building is in cooling mode, the rejected heat dumped into the ambient loop by the building's ETS may be utilized by another building's ETS in heating mode. This energy exchange is more effective when the buildings are more directly connected together within the network. However, better-connected 5GDHC systems require larger networks, more pumping energy, and lose more heat through the network pipes; therefore, larger, better-connected networks may not produce the optimal LCC or LCCO2 for a given district. Fig. 4 illustrates examples of these types of graphs for a district network.

In this study, the prototypical district consists of five buildings and a DES (Fig. 1). Therefore, six potential nodes exist in the network with the constraint that any network topology must include the DES as a node.

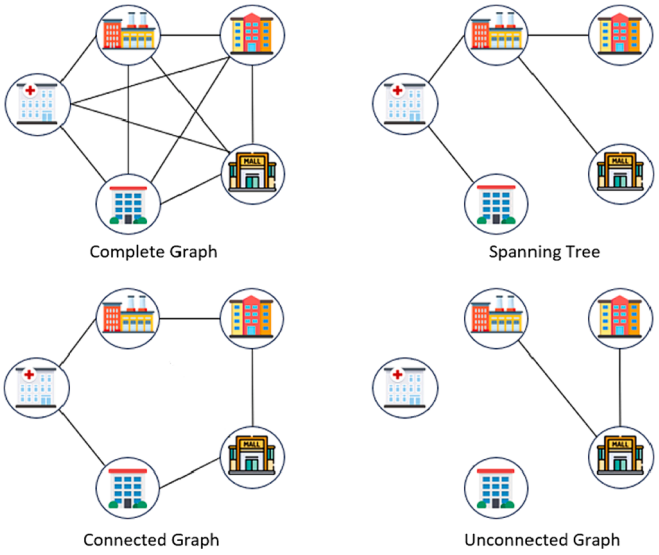

Fig. 4. Examples of different graphs for a five-node 5GDHC network (The prototypical district in this study is a six-node graph as the DES is included as a node).

Therefore, the smallest network topology consists of two nodes (DES and one building) connected by one pipe section. The largest network topology consists of six nodes (DES and five buildings) connected by 15 pipe sections. In the prototypical district, 30,770 possible network topologies exist for the selection of any subset of buildings in the district and the network configurations to connect them.

2.3. Life cycle cost

In this network topology optimization problem, costs for operating energy (electricity and gas), piping and trenching (investment cost), and price of CO_2 served as the LCC objective function.

$$LCC_{(30)} = \left(\sum_{t=0}^{30} m_{CO2,Op(t)} K_{CO2(t)} (1+ds)^{-t}\right) + (K_{ele} E_{ele} UPV_{ele}) + (K_{gas} E_{gas} UPV_{gas}) + K_{Invest} \quad (1)$$

where K_{Invest} is the capital investment cost of installing the network ($), K_{ele} is cost of electricity ($/kWh), K_{gas} is cost of gas ($/kWh), $K_{CO2(t)}$ is

cost of CO_2 ($/kg) during an individual year (see Appendix A), E_{ele} is annual electricity consumption (kWh), E_{gas} is annual gas consumption (kWh), UPV is uniform present value for the 30-year operating horizon, $m_{CO2,Op(t)}$ is the mass of CO_2 (kg) from operating over a given year (t), and ds is discount rate per year (3 %).

$$E_{ele} = E_{ele,DES} + E_{ele,pumping} + \sum_{i=0}^{N} E_{ele,ETS(i)} + \sum_{i=0}^{M-N} E_{ele,DX(i)} \quad (2)$$

where $E_{ele,DES}$ is the annual electricity consumption of the DES (kWh), $E_{ele,pumping}$ is the annual electricity consumption of the pumps throughout the network (kWh), $E_{ele,ETS}$ is the annual electricity consumption of an ETS in building (i) connected to the network (kWh), $E_{ele,DX}$ is the annual electricity consumption of a direct expansion cooling system in building (i) not connect to the network (kWh), N is the subset of buildings connected to the network, M is the total number of buildings in the prototypical district.

$$E_{gas} = \sum_{i=0}^{M-N} E_{gas,heater(i)} \quad (3)$$

where E_{egas} is the annual gas consumption for buildings not connected to the network (kWh), $E_{gas,heater}$ is the annual energy consumption of a gas heater in a building (i) not connected to the network (kWh).

$$m_{CO2,Op(t)} = E_{gas}C_{gas} + E_{ele}C_{ele(t)} \quad (4)$$

where C_{gas} is the CO_2 emissions factor of natural gas (constant over 30-year simulation horizon) ($kgCO_2e/kWh$), C_{ele} is the CO_2 emissions factor of electricity ($kgCO_2e/kWh$) for a given year (t).

2.4. CO_2 life cycle assessment

The LCA model calculates the equivalent CO_2 emissions ($kgCO_2e$) from the production of the piping materials, transportation of piping and trenching materials and the installation of the network (excavation, pipe installation and refill). The LCA was carried out in accordance with ISO14040:2016. The LCCO2 included the equivalent CO_2 emissions resulting from the production of materials ($m_{CO2,Mat}$), transport of materials, aggregates and soil ($m_{CO2,Tran}$), installation of the network ($m_{CO2,Inst}$) and the operation of the network ($m_{CO2,Op}$) over the 30-year operating horizon.

$$LCCO2_{(30)} = m_{CO2,Mat} + m_{CO2,Tran} + m_{CO2,Inst} + \sum_{i=0}^{30} m_{CO2,Op(t)} \quad (5)$$

2.4.1. Materials

The embodied CO_2 of the pipe materials takes into account the transport and processing of the raw ingredients based on typical supply chains and fuel mixes in the United States [31]. All other pipe material specifications were source from the pipe manufacturer [32].

The equivalent CO_2 emissions resulting from the production of the DHC pipe materials was calculated based on the associated embodied CO_2 ($kgCO_2e/kg$) of each material ($ECO2_{Mat(i)}$) and the respective mass of each material (m_M). This mass was calculated based on the length of the pipe (l), density of the material (ρ_M) and the thickness of the individual material in the DHC pipe based on the outer radius (r_o) and inner radius (r_i) of the material cross section (Fig. 5). Where the pipe wall, insulation and casing materials were high-density polyethylene (HDPE), polyurethane foam (PU foam) and low-density polyethylene (LDPE), respectively.

$$m_{CO2,Mat} = \sum_{i=1}^{3} ECO2_{Mat(i)} m_{Mat(i)} \quad (6)$$

$$m_{Mat(i)} = \pi l \rho_{Mat(i)} \left(r_o^2 - r_i^2\right)_{Mat(i)} \quad (7)$$

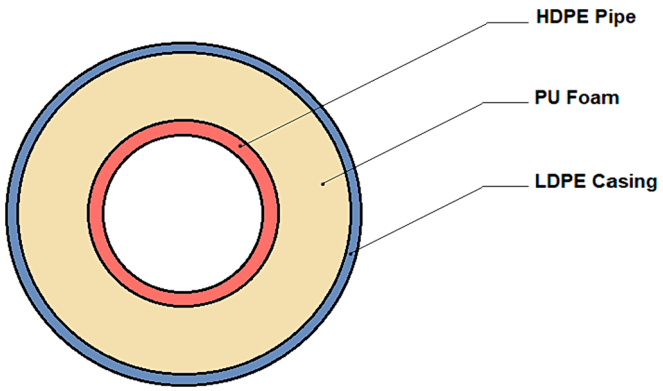

Fig. 5. DHC pipe (high-density polyethylene), insulation (polyurethane foam) and casing material (low-density polyethylene).

Table 2
LCA DHC pipe material parameters.

Parameter	Value
Pipe inner diameter (m)	0.16
Pipe wall thickness (HDPE) (m)	0.0146
Insulation thickness (PU Foam) (m)	0.045
Casing wall thickness (LDPE) (m)	0.01
Density HDPE (kg/m^3)	940
Density PU foam (kg/m^3)	65
Density LDPE (kg/m^3)	920
HDPE embodied CO_2 ($kgCO_2e/kg$)	1.897
PU Foam embodied CO_2 ($kgCO_2e/kg$)	4.035
LDPE embodied CO_2 ($kgCO_2e/kg$)	2.201

Table 2 displays the parameters used for calculating the equivalent CO_2 emissions resulting from the production of the DHC pipe materials.

2.4.2. Transport

All distances for material transportation were assumed constant (Fig. 6). The heavy goods vehicle (HGV) maximum capacity and fuel economy were based on a cognate study in Texas [33]. It was assumed the HGVs would return to the quarry/depot once drop off at the 5GDHC system location was completed. Complete combustion of the diesel consumed in transport was assumed with 99 % oxidization to form CO_2 [34].

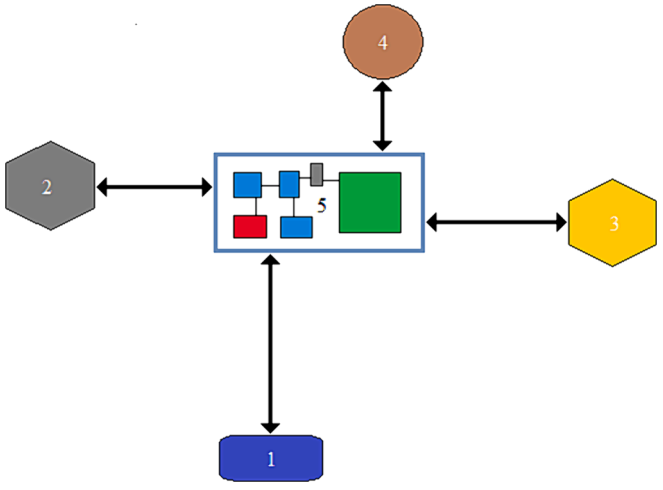

Fig. 6. Transportation of insulated DHC pipes, sand, gravel and removed earth from the 5GDHC system location. (1) DHC pipe supplier, (2) gravel quarry, (3) sand quarry, (4) earth disposal site, (5) 5GDHC system site.

Table 3
LCA transportation parameters.

Parameters	Value
Pipe transportation (single trip) (km)	250
Sand transportation (single trip) (km)	50
Gravel transportation (single trip) (km)	60
Earth for removal transportation (single trip) (km)	40
HGV max capacity (kg)	23,500
HGV fuel economy (l/km)	2.3
CO_2 from diesel combustion ($kgCO_2e/l$)	2.68

$$m_{CO2,Tran} = CC_{Diesel} F_{HGV} \left(D_{Sand} + D_{Gravel} + D_{Earth} + D_{Pipes}\right) \quad (8)$$

where CC_{Diesel} is the CO_2 of combustion for diesel ($kgCO_2e/l$), F_{HGV} is the HGV fuel economy (l/km) and D is the transported distance (km).

$$D_{material} = 2\left\lceil \frac{m_{mat}}{Cap_{HGV}} \right\rceil \quad (9)$$

where Cap_{HGV} is the maximum haulage capacity of the HGV (kg), m is the mass of the material.

Table 3 displays the parameters used for calculating the equivalent CO_2 emissions resulting from the transportation of DHC pipes, sand, gravel and removed earth from the 5GDHC system location.

2.4.3. Installation

The trench configuration and dimensions were based on guidelines provided by ASHRAE [35] and the pipe manufacturer [32]. The base of the trench has a gravel layer for percolation purposes. The pipes are surrounded by a heavy sand layer and the upper layer consists of non-rocky earth backfill (assumed to be recycled from excavation). Table 4 displays the corresponding dimensions for the DHC trench and pipe configuration in Fig. 7.

Excavator diesel consumption was based on a typical Caterpillar excavator and was assumed constant during operation [36]. Electricity consumed by power tools in the pipe installation phase was considered to be proportional to network length [18]. It was assumed electricity supply from the grid was not available and therefore a diesel generator was used. The CO_2 emissions factor of the electricity generated on site was based on a typical diesel generator [37]. The excavator bucket rotation rate was assumed to be low as the trenching was through an urban area. It was assumed the DHC pipes were disconnected and left in the ground after the 30-year operating lifetime of the network [38]. The CO_2 emissions associated with network installation were based on:

$$m_{CO2,Inst} = EF_{Gen} E_{Gen} + CC_{Diesel} F_{Exc} \left(\frac{V_{Tren}}{P_{Exc}}\right) \quad (10)$$

where EF_{Gen} is the CO_2 emissions factor of the generated electricity (kg/kWh), E_{Gen} is the electrical energy produced by the generator (kWh), F_{Exc} is the excavator fuel economy (l/hr), V_{Tren} is the total trench volume (m^3) and P_{Exc} is the excavator productivity rate (m^3/hr).

$$P_{Exc} = 60 R_B V_B \quad (11)$$

where V_B is the mean bucket fill volume (m^3) and R_B is the bucket rotation rate (RPM).

Table 4
5GDHC trench dimensions.

	Dimension (m)	Value
1.	Backfill layer depth	0.3
2.	Distance between conduits and gravel layer	0.15
3.	Distance between individual conduits	0.1
4.	Distance between conduits backfill layer	0.15
5.	Distance between conduits and trench walls	0.15
6.	Gravel layer depth	0.1

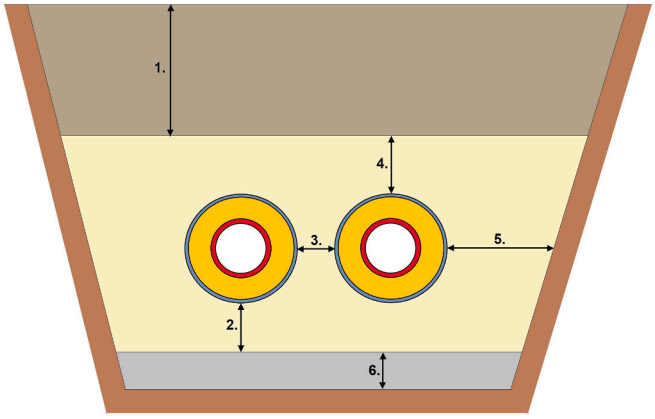

Fig. 7. Two pipe trenching configuration for a DHC network. In this diagram, pipe wall is red, insulation is orange, casing wall is blue, heavy sand backfill is yellow, gravel is grey, and backfill is brown.

Table 5
5GDHC network installation parameters.

Parameters	Value
Density of heavy sand (kg/m^3)	1,600
Density of gravel (kg/m^3)	1,350
Density of earth (kg/m^3)	1,440
Excavator bucket capacity (m^3)	0.2
Bucket rotation rate (RPM)	1.2
Excavator diesel consumption (l/hr)	45.38
Trench network length (m)	752
Electricity generator CO_2 emissions factor ($kgCO_2e/kWh$)	1.27
Electricity usage (power tools) (kWh/m)	0.3

Table 5 displays the parameters used for calculating the equivalent CO_2 emissions resulting from the installation of a 5GDHC network.

2.5. Waste heat recovery model

Two waste heat recovery methods for a 5GDHC system (Fig. 8) were considered: Method 1, termed "ambient loop pre-heating", involves pre-heating the ambient loop cool pipe before it enters the DES heat pump. Waste heat from the data center is recovered via a heat exchanger. If the ambient loop cool pipe is pre-heated from its cool setpoint temperature of 16 °C up to the warm loop setpoint temperature of 26 °C, DES input is not required during heating mode. If the ambient loop cool pipe is pre-heated to a temperature below 26 °C, DES input is required, however, the load on the heat pump is reduced, therefore less energy is consumed by the DES. The COP of the DES is not altered as the temperature differential between the evaporator and condenser is unchanged. Method 2, termed "DES evaporator heating" involves heating the DES evaporator using the recovered waste heat from the data center. This method increases the COP of the DES as the temperature differential between evaporator and condenser is lowered as the evaporator temperature is raised considerably by the waste heat, as ground-source water is utilized when no waste heat is available (4.4 °C mean ground-source temperature). Therefore, the energy required to meet the heating load is reduced.

The COP of the DES in heating mode ($COP_{Heating}$) depends on the temperature differential between the evaporator and condenser.

$$COP_{Heating} = \left(\frac{T_{Cond}}{T_{Cond} - T_{Evap}}\right)\eta \quad (12)$$

where T_{Cond} is the condensing temperature (K), T_{Evap} is evaporating temperature (K) and η is the Carnot effectiveness factor.

$$\theta_{DES,Heating} = (1 + COP_{Heating})\theta_{Comp} \quad (13)$$

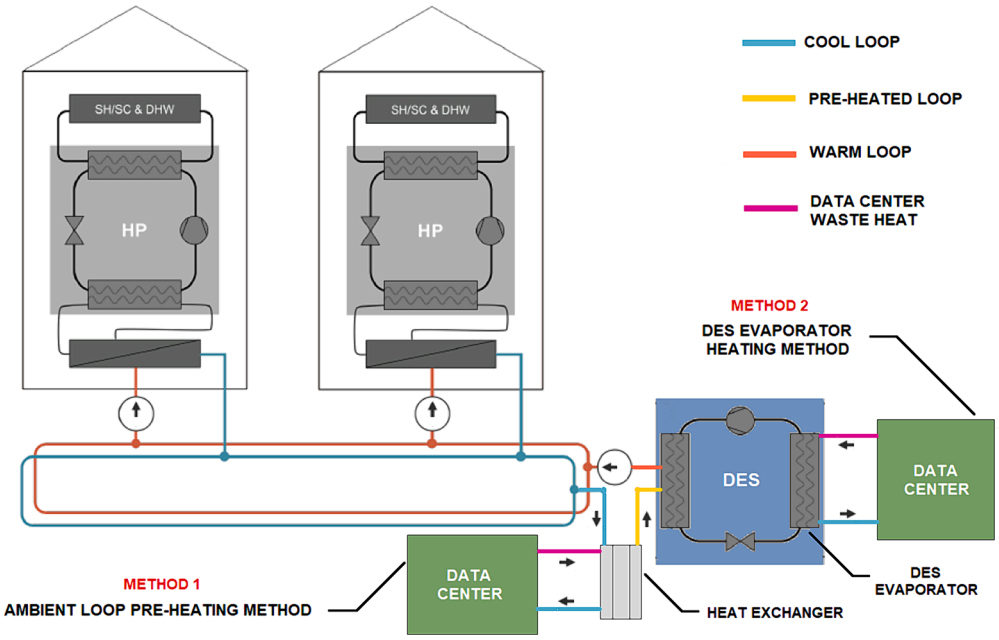

Fig. 8. 5GDHC network (heating mode) with data center heat recovery methods: (1) Ambient loop pre-heating, (2) DES evaporator heating (figure modified from [6]).

where $\theta_{DES,Heating}$ is the energy for heating required from the DES (J) and θ_{Comp} is the energy input to the DES compressor (J). The condenser temperature (T_{Cond}) is based on a static temperature offset (T_{Offset}) above the setpoint temperature of the warm ambient loop (T_{Wloop}) of 26 °C. The evaporator temperature (T_{Evap}) is a static offset below either the waste heat temperature from the data center (T_{waste}) or the ground source water temperature (T_{ground}), depending on the heat recovery method used. The static temperature offsets (Table 6) take into account the necessary temperature differentials (above the warm loop setpoint and below the cool loop setpoint) required for effective heat transfer to occur [6].

$$T_{Cond} = T_{Wloop} + T_{Offset} \tag{14}$$

$$T_{Evap} = \begin{cases} T_{ground} - T_{Offset}, Method\ 1 \\ T_{waste} - T_{Offset}, Method\ 2 \end{cases} \tag{15}$$

$$\theta_{Comp} = \frac{\theta_{DES,Heating}}{1 + COP_{Heating}} \tag{16}$$

$$\theta_{DES,Heating} = (T_{WLoop} - T_{Incoming})(m)(C_p) \tag{17}$$

$$T_{Incoming} = \begin{cases} T_{PreHeat}, Method\ 1 \\ T_{Cloop}, Method\ 2 \end{cases} \tag{18}$$

The heating energy output required from the DES heat pump ($\theta_{DES,Heating}$) is directly proportional to the temperature difference between the warm ambient loop setpoint (T_{Wloop}) and the incoming cool ambient loop temperature ($T_{Incoming}$). When the incoming cool ambient loop temperature is pre-heated using method 1, the loop temperature is raised to the pre-heat temperature ($T_{PreHeat}$). In method 2, the cool ambient loop is not pre-heated, therefore, the incoming cool ambient loop temperature remains at the cool loop setpoint temperature (T_{Cloop}) of 16 °C.

$$T_{PreHeat} = (T_{waste} - T_{CLoop})(\varepsilon) + T_{CLoop} \tag{19}$$

$$T_{PreHeat} \leq T_{WLoop} \tag{20}$$

The pre-heated ambient loop temperature is dependent on the cool ambient loop setpoint temperature (T_{CLoop}), the waste heat temperature from the data center (T_{waste}) and the heat exchanger effectiveness (ε). Where the maximum pre-heated cool ambient loop temperature is constrained not to exceed the warm loop setpoint temperature.

A DES output heating requirement of 100 (GJ) was selected for analysis. Typically, waste heat temperatures from air-cooled data centers range from 10 to 35 °C [39,40]. Direct contact liquid-cooled systems produce waste heat return temperatures greater than air-cooled systems and can be employed with air-cooling in a hybrid system. Liquid submerged cooling systems can produce waste heat return temperatures of up to 60 °C [40]. However, air-cooled and hybrid direct liquid- and air-cooled systems are currently the most common cooling methods employed in data centers. Also, 5GDHC systems are suited to utilizing low-grade waste heat. Therefore, we selected the lower and upper waste heat temperate limits of 10 – 40 °C as they were deemed to be most realistic. A heat exchanger effectiveness of 0.5 was deemed a suitable value for this application [41]. The remaining parameters in Table 6 were selected based on [28].

Empirical data were collected from the hybrid direct air- and liquid-cooling systems at the Energy System Integration Facility (ESIF) at the High-Performance Computing (HPC) data center located at the U.S. National Renewable Energy Laboratory (NREL) in Golden, Colorado. The hybrid cooling system has the capacity to produce approximately 1 MW of recovered heat from the air and water returns combined (for detailed information on this system please see [42,43]). Supply temperature, return temperature and cooling power were recorded at a one-minute time step for a 12-month period (September to August) for both

Table 6
Parameters for waste heat recovery analysis.

Parameter	Value
Warm ambient loop temperature setpoint (°C)	26
Condenser temperature offset (°C)	10
Evaporator temperature offset (°C)	10
Carnot effectiveness factor	0.5
Maximum waste heat temperature (°C)	40
Minimum waste heat temperature (°C)	10
Cool ambient loop temperature setpoint (°C)	16
Heat exchanger effectiveness	0.5
Ground return temperature (°C)	4.4

the air- and liquid-cooling systems. The waste heat database is available from the online data repository [44]. The performance of both systems was analyzed to assess the variability of return temperatures, seasonal variations, and the suitability for integration with the 5GDHC network. The results from this analysis are presented in Table 8.

2.6. Network piping and trenching cost

Fig. 9 displays the network piping and trenching cost for the studies summarized in Table B1, Appendix B. Currencies were converted to USD and inflation was accounted for in the intervening period (US Bureau of Labor Statistics). The mean and median costs for the studies in Fig. 9 were $636/m and $552/m, respectively. The piping and trenching cost for this study was selected from Allen, et al, [45] ($548/m for a 0.16 m diameter pipe) as this study is based on the same application.

2.7. Network topology simulation

Before the optimal network topologies could be selected, all possible network topologies ($top_{(all)}$) within the constraints (see Section 2.2.1) of the prototypical 5GDHC system in this study were first identified using equation (21).

$$top_{(all)} = 1 + \sum_{i=1}^{n-1} \binom{n-1}{i} \alpha(i+1) \tag{21}$$

where i buildings are connected to a network with a single DES, resulting in n connections on the network. α is the number of connected graphs with $(i+1)$ nodes. The single null case topology where all buildings use their independent HVAC systems (Table 1) and are not connected to the network is also included.

This resulted in 30,770 possible network topologies with 32 possible subsets of buildings connected to the network. The NREL HPC was used to simulate each network topology over the time horizon using the detailed 5GDHC Modelica model created by von Rhein, et al., [6] and further developed by Allen, et al., [28]. These simulations calculated all loads, temperatures, mass flow rates, heat loss, electricity consumption and gas consumption throughout the 5GDHC system for all network topologies. LCC and LCCO2 for each network topology were then calculated using the outputs of these simulations along with the outputs from the waste heat recovery model (Section 2.5) the LCA model (Section 2.4) and the scenario parameters (K_{Invest}, K_{ele}, K_{gas}, K_{CO2}, C_{ele}, C_{gas}, UPV, ds) (Section 2.3). As the Modelica simulations of the 5GDHC network topologies are not affected by the scenario parameters, these parameters can be independently changed, and LCC and LCCO2 recalculated without the requirement to re-run the Modelica simulations. This greatly reduced the computational expense associated with exploring multiple scenarios.

2.8. Multi-objective optimization and Pareto analysis

A multi-objective optimization algorithm was employed to find the optimal trade-offs between the environmentally and economically optimal network topologies for the five-building district. The algorithm employed an exhaustive method to search through all 30,770 possible network topologies (for a given scenario) and their corresponding LCC and LCCO2 values. A blended cost function (J) was used to explore the trade-offs between LCC and LCCO2 for a network topology (top) using the trade-off parameter (γ) [46].

$$Minimize: J_{(top)} = (\gamma)\left(LCCO2'_{(top)}\right) + (1-\gamma)\left(LCC'_{(top)}\right) \tag{22}$$

where $LCCO2'_{(top)}$ and $LCC'_{(top)}$ are the normalized LCCO2 (tCO_2e) and normalized LCC ($) for a given network topology, respectively.

$$LCCO2'_{(top)} = \frac{LCCO2_{(top)} - LCCO2_{(top\ min)}}{LCCO2_{(top\ max)} - LCCO2_{(top\ min)}} \tag{23}$$

where $LCCO2_{(top\ max)}$ and $LCCO2_{(top\ min)}$ are the topologies with the maximum and minimum LCCO2 values, respectively.

$$LCC'_{(top)} = \frac{LCC_{(top)} - LCC_{(top\ min)}}{LCC_{(top\ max)} - LCC_{(top\ min)}} \tag{24}$$

where $LCC_{(top\ max)}$ and $LCC_{(top\ min)}$ are the topologies with the maximum and minimum LCC values, respectively.

The yield ratio is a measure of the reduction in LCCO2 relative to the

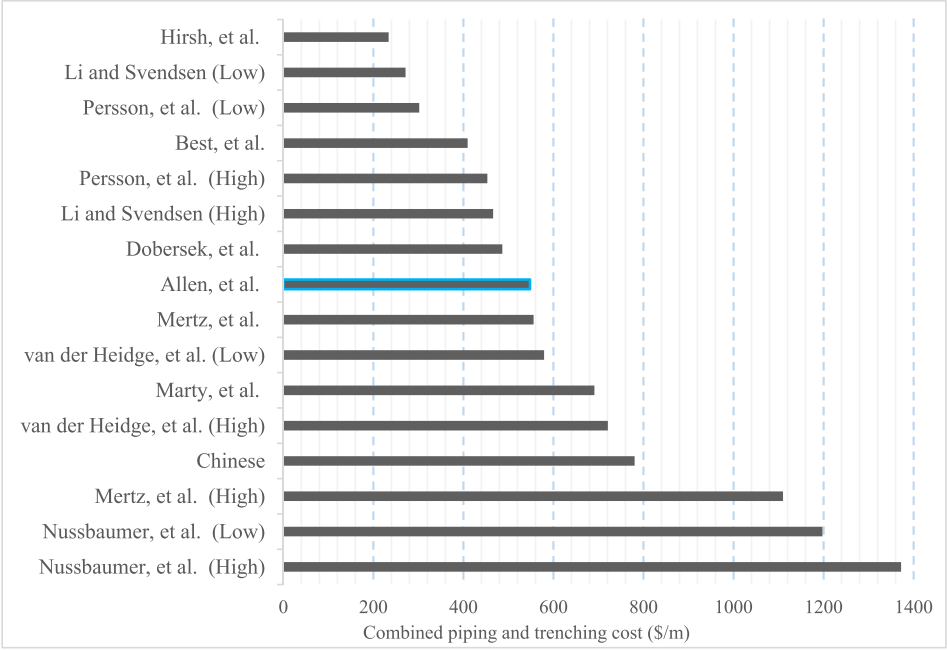

Fig. 9. Piping and trenching cost estimations for a 0.16 m diameter DHC pipe. The value used in this study is highlighted in blue. Low = the lower estimate limit and High = the higher estimate limit if the study used an estimated cost range. See table B1 for more information and citations for these studies.

increase in LCC for an optimal trade-off topology (*trade-off top*).

$$yield\ ratio_{(trade-off\ \ top)} = \frac{LCCO2_{(LCC_{(top\ \ min)})} - LCCO2_{(trade-off\ \ top)}}{LCC_{(trade-off\ \ top)} - LCC_{(top\ \ min)}} \quad (25)$$

where $LCC_{(\text{top min})}$ is the cost of the topology with the minimum LCC (economically optimal topology) and $LCCO2_{(LCC_{(\text{top min})})}$ is the LCCO2 produced by the $LCC_{(\text{top min})}$ topology.

In this study, the trade-off parameter (γ) was varied from 0 (economically optimal network topology) to 1 (environmentally optimal network topology) in steps of 0.05 to generate the Pareto front, which contained the set of Pareto optimal solutions [47,48], within the deterministically populated space of 30,770 network topologies for each scenario. The optimal trade-off (Pareto optimal) topologies in-between the environmentally and economically optimal topologies were selected within this Pareto front. This enabled the quantification of the yield ratio for selected topologies along the Pareto front (see Fig. 12).

2.9. Simulated scenarios

Four scenarios for multi-objective optimization and Pareto analysis were selected for this study (see Table 7). In each of these scenarios, the economic, environmental, and optimal trade-off network topologies were compared, and the yield ratios were calculated. Each scenario builds upon the previous scenario. The scenarios were compared to analyze the effects of adding a full LCA, waste heat recovery, varying CO_2 prices and CO_2 emissions factors.

Table 7
Scenarios for multi-objective analysis of optimal network topologies.

Scenario	Description
1. Operating CO_2	Pareto analysis of optimal 5GDHC network topologies (trade-off between LCC and LCCO2). Only operating CO_2 is considered in this scenario as a 5GDHC network operator will incur a carbon cost for only these CO_2 emissions.
2. Full LCA	In this scenario, LCCO2 is considered in the Pareto analysis. An LCA is added to the previous scenario to analyze the impact of the embodied CO_2 associated with the manufacturing, transport, and installation of the piping network.
3. Heat recovery	The availability of waste heat for utilization in the network is added to the previous scenario to quantify the effect that cost free, CO_2 neutral waste heat has on the selection of the optimal trade-off network topologies.
4. CO_2 analysis	Varying CO_2 prices and CO_2 emissions factors are added to the previous scenario. A sensitivity analysis is carried out to explore the effect of these variations on the optimal trade-off network topologies and the corresponding yield ratios and CO_2 offset costs.

All simulations were evaluated for a 30-year period (2020 – 2050), as this was deemed to be the maximum realistic lifetime for a 5GDHC network [10,49]. The cost of electricity (K_{ele}) and gas (K_{gas}) at the base year were 27.8 $/GJ and 6.48 $/GJ, respectively [28]. The UPV values for gas and electricity, CO_2 prices (K_{CO2}) and CO_2 emissions factors (C_{ele}) for the 2020 – 2050 simulation horizon were provided by the U.S. National Institute for Standards and Technology (NIST) [50] (see Appendix A). For simulations with waste heat recovery, the parameters from Table 6 were employed in the simulation with a waste heat supply temperature of 36.6 °C (see Section 3.1). As this recovered heat would have been otherwise dumped into the atmosphere if not recovered, we assume it is CO_2 neutral and supplied at no cost to the 5GDHC operator.

3. Results and discussion

This section presents the results of the waste heat recovery analysis (see Section 2.4), LCA results for the mean network topology length (see Section 2.3), and the multi-objective Pareto analysis of optimal network topologies for the four scenarios described in Table 7.

3.1. Waste heat recovery analysis

Fig. 10 displays the outputs of the waste heat recovery analysis. For the DES evaporator heating method (see Fig. 8), the COP (in heating mode) of the DES considerably increases as the temperature of the waste heat entering the evaporator rises while the condensing temperature remains static. This results in a much lower DES energy input for higher waste heat temperatures.

For the ambient loop pre-heating method (see Fig. 8), temperatures of 16 °C and less have no effect on the DES energy input. This is due to the setpoint temperature of 16 °C in the cool ambient loop, therefore no energy transfer from the waste heat can occur. However, once the waste heat temperature rises above this threshold, the DES energy input begins to reduce. The COP remains static as the evaporator and condenser

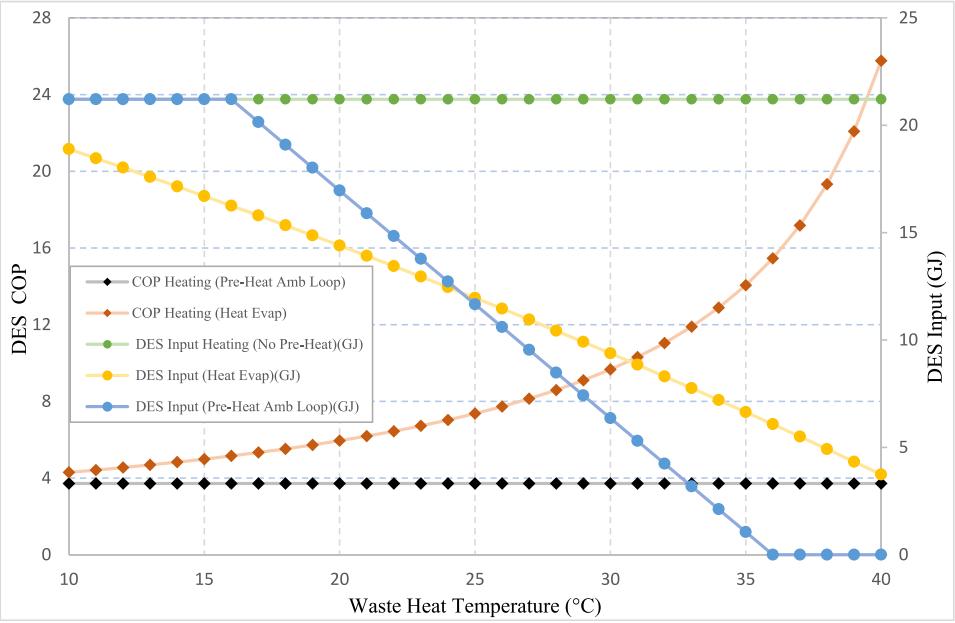

Fig. 10. DES COP and energy input for varying waste heat temperatures for both DES evaporator pre-heating and ambient loop pre-heating methods.

temperatures are constant, the pre-heating of the warm ambient loop reduces the load on the DES and, therefore, reduces the required energy input to the compressor. When a waste heat temperature of 36 °C or greater is available, the DES input energy drops to zero as the ambient loop is heated to its temperature setpoint by the waste heat and the DES is not required for heating.

When the waste heat temperature is less than 25 °C, the DES evaporator pre-heating method is more advantageous, while the ambient loop pre-heating method is more effective for waste heat temperatures greater than 25 °C. Please note, for situations where the waste heat temperature is 36 °C or greater, only the DES heating load is met. The energy consumption of the ETSs in the 5GDHC network operates as normal as the warm ambient loop setpoint temperature remains at 26 °C. Therefore, only a portion of the heating load can be provided by waste heat.

The effectiveness of the waste heat recovery may be further improved by combining the ambient loop pre-heating and the DES evaporator heating methods. In this combined method, remaining waste heat after ambient loop pre-heating would be supplied to the DES evaporator. This would increase the DES COP and further reduce the DES energy input. However, this combined method would only be advantageous for the application in this study if the temperature of the waste heat was less than 36 °C. Depending on the level of pre-heating achieved in the ambient loop, the increase in DES COP would not result in a substantial reduction in DES energy input for this application. Therefore, this combined method was not considered for this study. However, it may be suitable for future applications.

Table 8 displays the monthly mean and monthly standard deviation values for cooling power ($\dot{Q}$), supply temperature (T_S) and return temperature (T_R) for the hybrid air- and water-cooled HPC data center described in Section 2.4. The return temperatures for the liquid-cooled system are substantially higher than the air-cooled system, while the standard deviation in temperature is relatively lower for the liquid-cooled system. The mean annual return temperature for the liquid-cooled system is 36.6 °C. We can see across the 12-month period, there is very little variation in the mean return temperature, and during each month the standard deviation in return temperature is always less than 1 °C for the liquid-cooled system. The liquid-cooled system in this data center would be a highly suitable source of waste heat for the 5GDHC network in this study as it would provide a consistent supply of thermal energy at the required temperature range.

3.2. Network life cycle assessment

Table 9 displays the non-operational CO_2 emissions and associated LCA outputs from the construction of a 5GDHC network. The network specification and dimensions were based on Tables 2–5 in Section 2. The length of the network selected for this example (752 m) was the mean network length of all possible network topologies for the five buildings and DES presented in Section 2.1. The results show that installation accounted for the least CO_2 at 6.2 % of total non-operational CO_2 production, while transport accounted for 30.3 % and material manufacturing was largest at 63.5 %. The non-operational CO_2 produced per unit length of network (trenching and piping) was 130.3 $kgCO_2e/m$, for a 752 m long network. The CO_2 produced per unit length of network does not change relative to overall network length for manufacturing and installation. However, for transport, partial loading of the HGVs may occur based on the overall length of piping required and the haulage capacity of the HGVs. This results in minor differences in CO_2 produced by transportation of the insulated DHC pipes for network topologies of different lengths.

Table 8
Monthly mean cooling power, supply temperature and return temperature for both air- and liquid-cooling systems. Standard deviation in parenthesis.

Month	Air-cooled			Liquid-cooled		
	$\dot{Q}_{Air}$(kW)	$T_{Air,S}$(°C)	$T_{Air,R}$(°C)	$\dot{Q}_{Water}$(kW)	$T_{Water,S}$(°C)	$T_{Water,R}$(°C)
Sep	159.9 (9.21)	21.3 (0.56)	30.1 (0.49)	623.6 (81.79)	23.3 (0.35)	35.9 (0.68)
Oct	162 (12.32)	21 (0.5)	30.3 (0.47)	695.3 (71.33)	22.8 (0.33)	36.5 (0.65)
Nov	173.3 (15.29)	20.8 (1.45)	29.9 (1.68)	706 (85.85)	22.5 (0.44)	36.7 (0.8)
Dec	164.3 (8.67)	20.5 (0.66)	30.1 (0.57)	728.7 (43.99)	22.3 (0.48)	36.9 (0.4)
Jan	154.8 (14.69)	20.4 (1.05)	30.1 (1.33)	757.2 (80.06)	22 (1.34)	36.9 (0.81)
Feb	168.4 (9.85)	20.4 (1.67)	30.8 (2.1)	771.2 (41.6)	22.6 (0.4)	36.9 (0.59)
Mar	172.4 (9.08)	20.7 (1.05)	31.1 (1.33)	787.1 (31.78)	23 (0.29)	36.6 (0.4)
Apr	170.4 (22.48)	20.3 (3.53)	30.1 (4.46)	704.4 (110.49)	22.8 (1.35)	35.8 (0.98)
May	173.8 (18.7)	20.7 (0.51)	31 (0.69)	733 (48.03)	22.4 (1.4)	36.8 (0.43)
Jun	177.2 (9.08)	21 (0.46)	31.2 (0.53)	726.5 (42.68)	23 (0.32)	36.7 (0.39)
Jul	177.8 (7.53)	21.4 (0.37)	31.5 (0.63)	707.2 (95.58)	23.5 (0.31)	36.5 (0.86)
Aug	179.2 (5.84)	21 (0.7)	31.1 (0.92)	731.9 (46.18)	23.1 (0.31)	36.6 (0.54)

Table 9
LCA outputs for a 752 m network with 0.16 m diameter pipe.

5GDHC network life cycle assessment outputs			
CO_2 emissions		**Materials consumed**	
Installation CO_2 ($kgCO_2e$)	6,055	Sand (kg)	334,987
Transport CO_2 ($kgCO_2e$)	29,710	Gravel (kg)	70,983
Material CO_2 ($kgCO_2e$)	62,216	Earth for removal (kg)	529,399
Total network CO_2 ($kgCO_2e$)	97,982	HDPE (kg)	11,323
Network CO_2 per length ($kgCO_2e/m$)	130.3	PU foam (kg)	3,237
		LDPE (kg)	12,573
Transportation			
Pipe transportation (km)	1000	**Fuel consumption**	
Sand transportation (km)	1500	Total electricity consumption (kWh)	226
Gravel transportation (km)	480	Transport diesel consumption (l)	11,086
Earth for removal transportation (km)	1840	Trenching diesel consumption (l)	2153
Total HGV haulage distance (km)	4820	Total diesel consumption (l)	13,239

3.3. Multi-objective Pareto analyses

In this section the results of the multi-objective analyses for the four scenarios described in table 7 are presented.

3.3.1. Scenario 1 operating CO_2

In this scenario only the CO_2 associated with operating the 5GDHC network is taken into consideration; a full LCA is not employed. Therefore, the CO_2 associated with constructing the network is ignored. Fig. 11 compares, for this scenario, the economically optimal (lowest possible LCC) and the environmentally optimal (lowest possible CO_2 emissions) network topologies based on CO_2 emissions, LCC, network length and number of pipe sections.

The environmentally optimal network topology consisted of a 955 m network with nine pipe sections and all buildings connected, while the economically optimal topology had only one building connected to the network (hospital) via a 112 m one pipe network (at least five pipe sections and a minimum total network length of 329 m are required to create an MST, and therefore connect all buildings). (Note that the LCC, defined in Eq. (1), includes a CO_2 price.) The environmentally optimal network topology reduced CO_2 emissions by 11.9 % but increased LCC by 16.5 % relative to the economically optimal network.

The environmentally optimal network topology was not the best-connected network topology. The largest and best-connected network topology (fully connected) consisted of 15 pipe sections with a total network length of 1470 m (complete graph, see Fig. 4). Larger network topologies (topologies consisting of more than nine pipe sections) were not selected as the environmentally optimal solution as the additional pipe sections (directly connecting buildings together and taking advantage of load diversity) did not produce a reduction in heating and cooling loads on the network (and thus energy use by the DES heat pump) large enough to offset the energy lost due to the extra heat loss and pumping energy required.

The optimal trade-off network topologies that lie between the economically and environmentally optimal network topologies are displayed in Fig. 12. The optimal trade-off network topology (network topology that delivers a CO_2 reduction for the best value) was deemed to be $\gamma = 0.65$, which produced a yield ratio of 1.97, and resulted in a CO_2 offset cost of 121 \$/tCO_2e relative to the economic optimum.

As the trade-off parameter γ is incrementally increased from 0 to 1, thus increasing the weight assigned to CO_2 emissions, there is a monotonic increase in network length and decrease in gas consumption. At $\gamma = 0.65$, gas usage is eliminated as all buildings become connected to the network and therefore, are fully electrified. The electricity consumption monotonically increases up to $\gamma = 0.9$, where it slightly decreases due to the better thermal connectivity of the larger network topologies (up to nine pipe sections) for $\gamma = 0.95$ and $\gamma = 1$ (see Fig. 13).

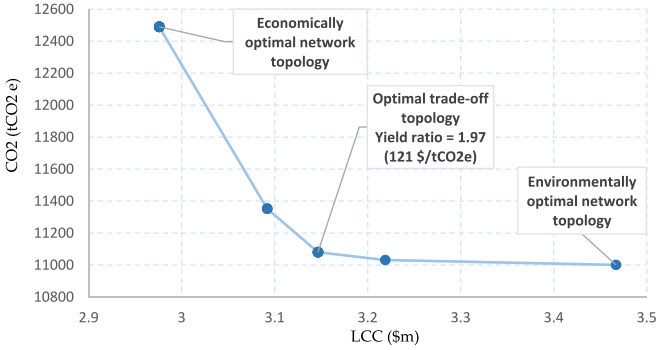

Fig. 12. Pareto trade-off analysis between CO2 and LCC for Pareto optimal network topologies for scenario 1. The economic, environmental, and optimal trade-off network topologies are labeled.

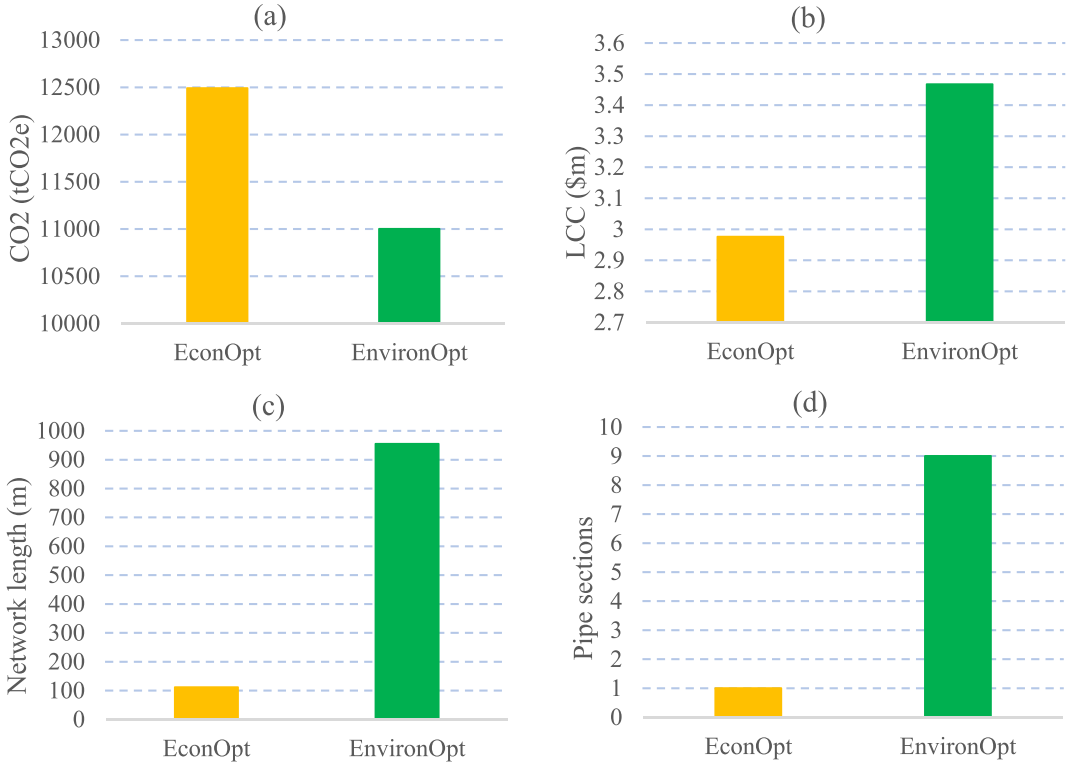

Fig. 11. Comparison of the economically optimal (EconOpt) and the environmentally optimal (EnvironOpt) network topologies for (a) CO2, (b) LCC, (c) network length, (d) number of pipe sections in the network.

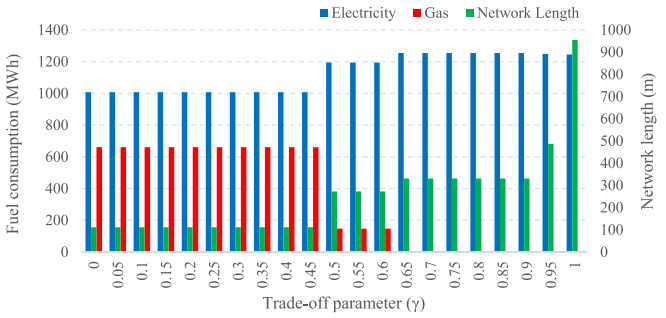

Fig. 13. Optimal network topology properties for trade-off parameter values (γ) from 0 to 1, and gas and electricity consumption and network length for scenario 1.

3.3.2. Scenario 2 full life cycle assessment

In this scenario the embodied CO_2 (manufacture, transport and installation) of the network is included with the operating CO_2 to consider the LCCO2 of the 5GDHC system.

The economically optimal network remained the same as scenario 1 as the costs did not change. However, the environmentally optimal network changed to 487 m in length comprising of six pipe sections and five buildings connected. This reduction in network size relative to scenario 1 is due to the consideration of the network's embodied CO_2. The additional CO_2 associated with building a larger network with greater than five pipe sections outweighed the CO_2 offset from the energy savings a better-connected network would produce.

The best trade-off optimal network topology was deemed to be $\gamma = 0.65$ (Fig. 14), which produced a yield ratio of 1.93 (Fig. 15), and resulted in a CO_2 offset cost of 123 $/tCO$_2$e.

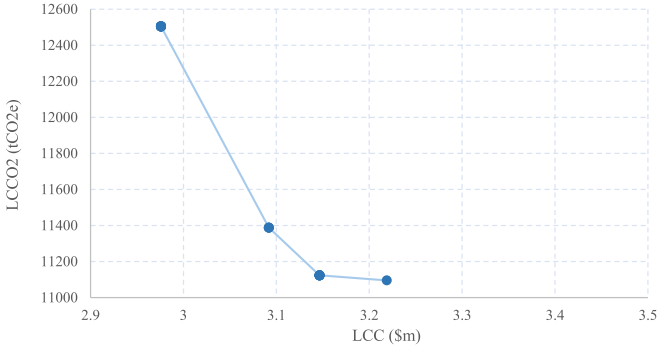

Fig. 14. Pareto trade-off analysis between LCCO2 and LCC for Pareto optimal network topologies for scenario 2. The horizontal axis is scaled relative to Fig. 12 for comparative purposes.

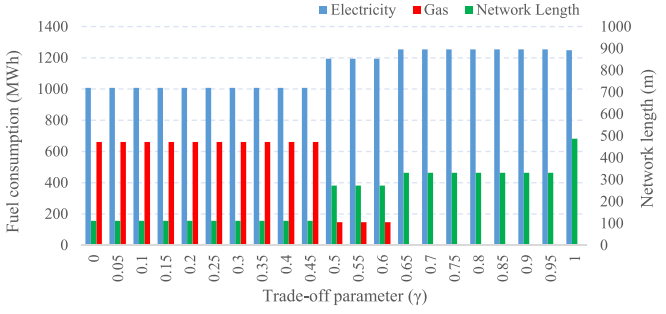

Fig. 15. Optimal network topology properties for trade-off parameter values (γ) from 0 to 1. Gas and electricity consumption and network length for scenario 2.

3.3.3. Scenario 3 waste heat recovery

In this scenario the full LCCO2 for the network is considered along with waste heat from a data center at 36.6 °C (see Section 3.1) recovered using the ambient loop pre-heating method, which was found to be preferable in terms of energy performance based on the waste heat supply temperature (see section 2.5). Therefore, in this scenario 100 % of the DES heating load is supplied using waste heat.

The addition of waste heat recovery from the data center made a substantial impact on the trade-off relationship between the economically optimal and the environmentally optimal network topologies. The best trade-off optimal network topology produced a LCCO2 reduction of 11.6 % for a corresponding LCC increase of 1.2 % resulting in a yield ratio of 9.34 (Fig. 16) and CO_2 offset cost of 25 $/tCO$_2$e.

In comparison to scenario 2, the environmentally optimal network topology increased in size with the inclusion of waste heat recovery (955 m network with nine pipe sections). Larger networks with additional pipe sections (more than five) became environmentally viable even with the embodied CO_2 of the network considered. When compared to scenario 2, we can see the optimal trade-off topologies became better-connected and used less gas as γ was incrementally increased to 1 (Fig. 17). This is explained by the availability of free, CO_2 neutral heat which makes the adoption of larger, better-connected networks more viable. While the addition of waste heat recovery had a substantial effect on the optimal trade-off topologies, it did not have a major impact on the net CO_2 savings. The LCCO2 produced by the environmentally optimal network topology in scenario 3 is 6 % lower than the environmentally optimal network topology in scenario 2. This is because the DES consumes only 21 % of the energy required for heating. The rest is consumed by the ETS heat pumps in each building connected to the network. Waste heat had no effect on the ETS heat pumps' energy consumption as the temperature of the ambient loop warm pipe remained at 26 °C. The DES energy consumption for heating,

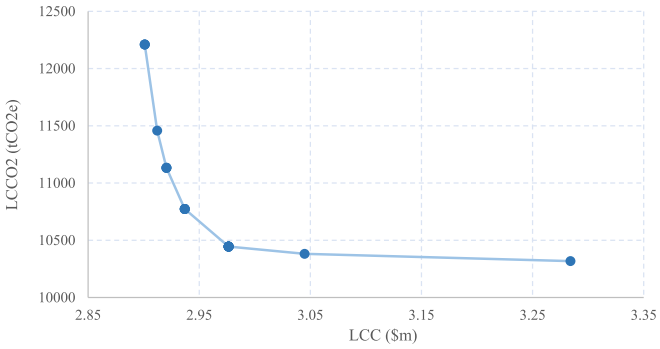

Fig. 16. Pareto trade-off analysis between LCCO2 and LCC for Pareto optimal network topologies for scenario 3.

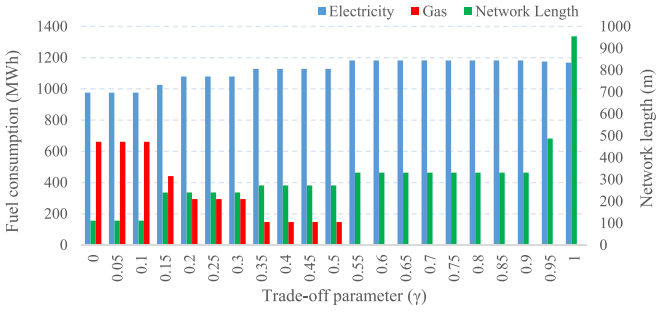

Fig. 17. Optimal network topology properties for trade-off parameter values (γ) from 0 to 1, and gas and electricity consumption and network length for scenario 3.

typically accounts for only 6 % of the total energy consumption for a given 5GDHC network topology with all buildings connected (DES energy consumption for heating and cooling of the ambient loop, ETS energy consumption for heating and cooling the buildings connected to the network, and energy required for pumping).

3.3.4. Scenario 4 CO_2 case analysis

In this scenario, the CO_2 properties of the electricity were varied, and the results analyzed. Two different CO2 cases were employed. In the "Medium CO_2 Case" the price of CO_2 tracks the medium CO_2 price scenario presented by NIST and the corresponding CO_2 emissions factors between 2020 and 2050 [42]. In the "High CO_2 Case" the price of CO_2 tracks the high price CO_2 scenario from NIST and the corresponding CO_2 emissions factors [42] (see Fig. A1 for a graphical presentation of these scenarios). The "low" CO_2 price and corresponding emissions factors forecasted by NIST were not used in this simulation as this scenario was very similar to the Medium CO_2 Case and therefore, the results would only vary slightly. NIST's joint future scenarios for the trajectory of a carbon price and corresponding electricity emissions factors are intended to reflect the expected effects of a CO_2 price incentivizing the use of cleaner electricity sources. Note, the Medium CO_2 Case was also employed for scenarios 1, 2 and 3 as it was deemed to be the most reasonable option for future projections. In scenario 4, the CO_2 emissions factor of the electricity in the base year was varied in steps (100 %, 75 %, 50 %, 25 %, 0 %) that were relative percentages of the base CO_2 emissions factor (625 kg/MWh). These variations were introduced as the CO_2 emissions factor of electricity can vary based on location and the availability of local renewable energy sources. The availability of the waste heat in scenario 3 is also assumed for all simulations in scenario 4.

Table 10a displays the results for the economically optimal network topologies for varying electricity CO_2 properties under the Medium and High CO_2 Cases (price and emissions factors). In the Medium CO_2 Case, the cost optimal network topologies when electricity CO_2 emissions factors were greater or equal to 50 % (0.3125 kg/kWh) of the base emissions factor had only one building connected to the network (one pipe section connecting the hospital to the DES). However, when electricity CO_2 emissions factors were less than 50 %, the number of buildings connected to the network substantially increased. Under the High CO_2 Case, far more buildings were connected to the network in comparison to the Medium CO_2 Case, and when electricity CO_2

Table 10
Economic, trade-off and environmental optimal network topology details for varying CO_2 scenarios and electricity CO_2 emissions factor.

(a) Economically Optimal Network Topologies

CO_2 Case[1]	Elec CO_2 EF Base Yr[2] (%)	Network Length (m)	Buildings[3]	Pipes[4]	TEC[5] (MWh)	TGC[6] (MWh)	LCC ($m)	LCCO2 (tCO_2e)
Medium	100	111.52	1	1	975.86	661.11	2.90	12225.19
	75	111.52	1	1	975.86	661.11	2.82	10069.98
	50	111.52	1	1	975.86	661.11	2.74	7914.78
	25	240.55	3	3	1079.25	294.44	2.65	4013.71
	0	272.78	4	4	1128.86	147.50	2.55	836.47
High	100	272.78	4	4	1128.86	147.50	3.38	9750.58
	75	272.78	4	4	1128.86	147.50	3.19	7522.06
	50	272.78	4	4	1128.86	147.50	2.99	5293.53
	25	331.12	5	5	1182.34	0.00	2.78	2377.25
	0	331.12	5	5	1182.34	0.00	2.57	43.14

(b) Optimal Trade-off Network Topologies

CO_2 Case	Elec CO_2 EF Base Yr (%)	Network Length (m)	Buildings	Pipes	TEC (MWh)	TGC (MWh)	LCC ($m)	LCCO2 (tCO_2e)
Medium	100	272.78	4	4	1128.86	147.50	2.94	10808.99
	75	272.78	4	4	1128.86	147.50	2.84	8315.79
	50	272.78	4	4	1128.86	147.50	2.75	5822.68
	25	272.78	4	4	1128.86	147.50	2.65	3329.57
	0	331.12	5	5	1182.34	0.00	2.57	43.14
High	100	331.12	5	5	1182.34	0.00	3.41	9379.55
	75	331.12	5	5	1182.34	0.00	3.20	7045.45
	50	331.12	5	5	1182.34	0.00	2.99	4711.35
	25	331.12	5	5	1182.34	0.00	2.78	2377.25
	0	331.12	5	5	1182.34	0.00	2.57	43.14

(c) Environmentally Optimal Network Topologies

CO_2 Case	Elec CO_2 EF Base Yr (%)	Network Length (m)	Buildings	Pipes	TEC (MWh)	TGC (MWh)	LCC ($m)	LCCO2 (tCO_2e)
Medium	100	954.70	5	9	1167.96	0.00	3.28	10442.24
	75	486.91	5	6	1175.17	0.00	2.94	7849.62
	50	486.91	5	6	1175.17	0.00	2.85	5254.22
	25	331.12	5	5	1182.34	0.00	2.67	2654.36
	0	328.88	5	5	1183.34	0.00	2.58	42.85
High	100	486.91	5	6	1175.17	0.00	3.47	9343.28
	75	486.91	5	6	1175.17	0.00	3.27	7023.32
	50	486.91	5	6	1175.17	0.00	3.06	4703.36
	25	331.12	5	5	1182.34	0.00	2.78	2377.25
	0	328.88	5	5	1183.34	0.00	2.58	42.85

[1] CO_2 Case refers to both the CO_2 price of the fuel and the CO_2 emissions factors presented in Appendix A. [2]Electricity CO_2 emissions factor relative to the base year. [3]Buildings = number of buildings connected to the network. [4]Pipes = number of pipe sections in the network. [5]TEC = total electricity consumption. [6]TGC = total gas consumption.

Table 11
Yield Ratios and CO_2 offset cost for varying CO_2 scenarios.

CO_2 Case[1]	Elec CO_2 EF[2] (%)	Increase in LCC (%)	Reduction in LCCO2 (%)	Yield Ratio	Cost[3] ($/t$CO_2$e)
Medium	100	1.24	11.59	9.34	25.41
	75	0.82	17.42	21.36	13.10
	50	0.36	26.43	72.45	4.77
	25	0.14	17.05	117.79	5.60
	0	0.83	94.84	113.71	26.84
High	100	0.66	3.81	5.78	60.08
	75	0.40	6.34	15.66	27.03
	50	0.12	11.00	94.44	5.97
	25	0.00	0.00	0.00	NA
	0	0.00	0.00	0.00	NA

[1] CO_2 Case refers to both the CO_2 price of the fuel and the CO_2 emissions factors presented in Appendix A. [2]Electricity CO_2 emissions factor relative to the base year. [3]CO_2 offset cost.

emissions factors were less than 50 % of the base CO_2 emissions factor, the economically optimal network topology had all buildings connected using the minimum number of pipe sections.

Table 10b displays the results for the optimal trade-off network topologies for varying electricity CO_2 emissions factors under the Medium and High CO_2 Cases. The optimal trade-off network topologies under the Medium CO_2 Case had four to five buildings connected, while all optimal trade-off networks had five buildings connected for the High CO_2 Case. These optimal trade-off network topologies produced some very high yield ratios and low CO_2 offset costs (Table 11).

Table 10c displays the results for the environmentally optimal network topologies for varying electricity CO_2 emissions factors under the Medium and High CO_2 Cases. In the Medium CO_2 Case, we can see the environmentally optimal network topology was a large, well-connected network (five buildings connected, nine pipe sections, 954.7 m network length). However, as the base CO_2 emissions factors were decreased, the environmentally optimal network topology became smaller and less connected. This may seem counter intuitive, however as the CO_2 emissions factors of the electricity were reduced, the embodied CO_2 of the network became proportionately larger, relative to the operating CO_2. When the CO_2 emissions factor for the electricity was reduced to 0, the embodied CO_2 of the network became the only CO_2 source and therefore equaled the LCCO2. In this instance, the environmentally optimal network topology still had all five buildings connected but using the shortest possible network topology (five pipe sections, 328.88 m network length) which was the MST.

In the high CO_2 case, the same network topology (five buildings connected, five pipe sections, 331.12 m network length) was the optimal trade-off topology for all electricity CO_2 emissions factors (second shortest network topology after the MST). Interestingly, this same topology was both the economically and environmentally optimal network topology when the CO_2 emissions factors equaled 25 % of the base case (0.156 kg/kWh). This result is particularly interesting as many countries currently have CO_2 prices equal to, and well above the High CO_2 Case in this simulation [51] and electricity CO_2 emissions factors below 25 % of the base case in his study [52].

Table 11 displays the yield ratios and CO_2 offset costs for varying CO_2 scenarios. The yield ratios are based on the percentage reduction in LCCO2 achieved relative to the percentage increases in LCC required to select the optimal trade-off network topology. As can be seen in Table 11, there were substantial reductions in LCCO2 available for very modest increases in LCC. The CO_2 offset cost represents the cost of offsetting CO_2 through selection of the optimal trade-off network topology instead of the economically optimal network topology. Note, while the cost of emitting CO_2 was already accounted for through CO_2 prices (Fig. A1), the CO_2 offset cost presents the opportunity to offset additional CO_2 for a further investment cost. When CO_2 emissions factors are high, CO_2 offset costs are higher and yield ratios lower, as offsetting CO_2 with a 5GDHC system is more difficult with CO_2 intensive electricity.

The impact of installing a 5GDHC network to replace gas heating was lowered when the electricity running the network had a high CO_2 emissions factor. However, the CO_2 offset cost rose again for the Medium CO_2 Case when CO_2 emissions factors were very low. The economically optimal network topology moved closer to the environmentally optimal network topology when CO_2 emissions factors were reduced. Therefore, less opportunity existed to offset CO_2 through increasing the size and connectivity of the network. Also, the embodied CO_2 of the network plays a greater role in the LCCO2 in this situation, leading to less opportunity for finding low-cost CO_2 offsets through greater network connectivity. In the High CO_2 Case, a similar dynamic was observed. However, CO_2 offset opportunities were not available when CO_2 emissions factors are very low. This was due to the convergence of the economically and environmentally optimal network topologies for very low CO_2 emissions factors in the high CO_2 case. In other words, no opportunity existed to further offset CO_2, therefore the yield ratio went to zero, since the economic and environmental optima were already coincident.

Overall, we can see low CO_2 offset costs though the selection of the optimal trade-off network topology in Table 11. The CO_2 offset costs for the medium CO_2 case are far lower than most existing CO_2 prices in developed countries [51] and much lower than the social cost of emitting CO_2 in the U.S. which is estimated to be between 44 and 413 $/t$CO_2$e [53].

3.4. General discussion

The temperature of the waste heat available determines which recovery method is most suitable. When the waste heat temperature is less than 25 °C, the DES evaporator heating method is more effective. For the ambient loop pre-heating method, available waste heat with a temperature of 36 °C or above supplied all the energy required to heat the ambient loop to the setpoint temperature of 26 °C. Therefore, in scenarios where large amounts of high temperature (>36 °C) waste heat are available, the selection of a higher ambient loop warm pipe setpoint temperature is preferable as it would take advantage of high temperature waste heat and reduce the energy consumption of the ETSs in the network as the COP of the individual heat pumps in the ETSs would increase due to higher evaporating temperatures resulting from the warmer ambient loop. Experiments using liquid submerged cooling systems for the NREL HPC produced steady state water return temperatures of up to 51.7 °C [54]. The ambient loop setpoints for the 5GDHC system in this study could be optimized for higher waste heat temperatures. Temperate waste heat from other industrial applications could be integrated with the 5GDHC system in this study depending on temperature range, proximity to the network, variance in return temperature and power output. The waste heat data utilized in this study and the results from the summary analysis in Table 8 are available through an online data repository [44].

When embodied CO_2 was ignored and only operating CO_2 was considered, the environmentally optimal network topology was not a fully connected network of 1469 m with the maximum number of pipe

sections (15), but instead, a 955 m network with nine pipe sections produced the minimum operating CO_2. The addition of extra pipe sections beyond nine did not result in large enough energy savings in heating and cooling required to offset the extra energy required for pumping and energy lost via conduction in the extra pipe sections. The inclusion of embodied CO_2 through a full LCA reduced the size of the environmentally optimal network topology to 487 m with six pipe sections and all buildings still connected. This result showed the embodied CO_2 of a 5GDHC network should be considered when selecting the most suitable topology from an environmental perspective.

The addition of waste heat recovery resulted in a moderate LCCO2 reduction (6 %). However, the availability of this waste heat resulted in larger, better-connected networks becoming more economically and environmentally feasible. It also substantially increased the yield ratio (from 1.93 to 9.34) and created cheaper CO_2 offsets (from \$123/tCO_2e down to \$25/tCO_2e) for the optimal trade-off network topologies. In a network configuration with higher waste heat supply temperatures and higher ambient loop setpoint temperatures, there would be greater potential for waste heat utilization as waste heat would reduce energy use associated with the ETS heat pumps, which meet the majority of the heating load in this 5GDHC application.

The economically optimal and optimal trade-off network topologies (Tables 10a and 10b) were either MSTs or the next shortest network topology. These topologies connected the viable number of buildings to the network using the shortest, or near-shortest network. Adding additional pipe sections beyond a spanning tree to improve thermal connectivity was never selected for economically optimal or optimal trade-off network topologies. These results concur with previous studies [28,45], were the extra investment cost associated with larger, better-connected networks was not economically viable. However, when selecting the environmentally optimal network topology, larger, better-connected network topologies with additional pipe sections beyond that of the MST were selected when the CO_2 emissions factors were greater or equal to 50 % (Table 10c). The improved thermal connectivity of these larger networks resulted in reduced operating CO_2 (via reduced electricity consumption) which more than offset the embodied CO_2 associated with installing the larger network, therefore, reducing the LCCO2. However, when the CO_2 emissions factors of the electricity were less than 50 %, the environmentally optimal network topologies were either the MST or the next shortest network topology.

The CO_2 price and emissions factor of electricity had a substantial impact on the optimal network topology. All simulations with the High CO_2 Case resulted in optimal network topologies with four or five buildings connected. This demonstrated the importance of adequate CO_2 pricing for the future viability of 5GDHC networks, and the importance of CO_2 pricing in making this emissions reduction measure cost-effective.

Selection of the optimal trade-off network topologies produced very high yield ratios. The CO_2 offset costs associated with these networks were very low. This may present interesting investment opportunities for offsetting CO_2 emissions using 5GDHC systems.

4. Conclusions

We conclude this study by addressing the questions presented in Section 1:

- The inclusion of embodied CO_2 through a full LCA had a substantial impact on the selection of the environmentally optimal and optimal trade-off network topologies. When selecting a 5GDHC network based on LCCO2, a full LCA is necessary.
- The ambient loop pre-heating method was found to be the most effective waste heat recovery method for the 5GDHC network in this application due to the available waste heat temperature (36.6 °C). However, if the waste heat temperature was less than 25 °C, the DES evaporator heating method would have been selected. The utilization of waste heat though the ambient loop pre-heating method resulted in a LCCO2 reduction of 6 %. However, different network configurations with higher supply temperatures could have offered more potential for the utilization of waste heat.
- The environmentally optimal network topology was not a fully connected network, or even close to a fully connected network under any of the simulated scenarios. The extra CO_2 emissions resulting from the installation of larger networks and the extra electricity consumption due to additional pumping energy and heat loss through the extra pipe sections outweighed the benefits produced by a better-connected network.
- The MST or the next shortest network topology were the optimal trade-off network topologies selected. Substantial LCCO2 savings could be achieved through relatively small increases in LCC. Yield ratios from 5.78 to 117.79 were identified with CO_2 offset costs ranging from 4.77 to 60.08 (\$/tCO_2e). The results showed relatively cheap CO_2 offset opportunities for the optimal trade-off network topologies selected in many scenarios.
- The integration of waste heat resulted in larger, better-connected networks being selected as the optimal trade-off topology. It also substantially increased yield ratios and reduced CO_2 offset costs.
- CO_2 prices and CO_2 emissions factors had a substantial impact on the optimal trade-off topologies. When high CO_2 prices were included, all the buildings were connected to the optimal trade-of network topologies. This demonstrated the importance of CO_2 pricing for the future viability of 5GDHC networks, and the importance of CO_2 pricing in incentivizing this emissions reduction opportunity.

Declaration of competing interest

The authors declare that they have no known competing financial interests or personal relationships that could have appeared to influence the work reported in this paper.

Data availability

The data that has been used is confidential.

Acknowledgements

The authors would like to thank David Sickinger of NREL for his assistance in providing information and data relating to the ESIF HPC, and also Kim Trenbath and Marcus Bianchi of NREL for their input to this study. Fig. 4 was designed using images sourced from flaticon. This research was supported by the USA-Ireland Fulbright Scholarship Award.

Appendix A

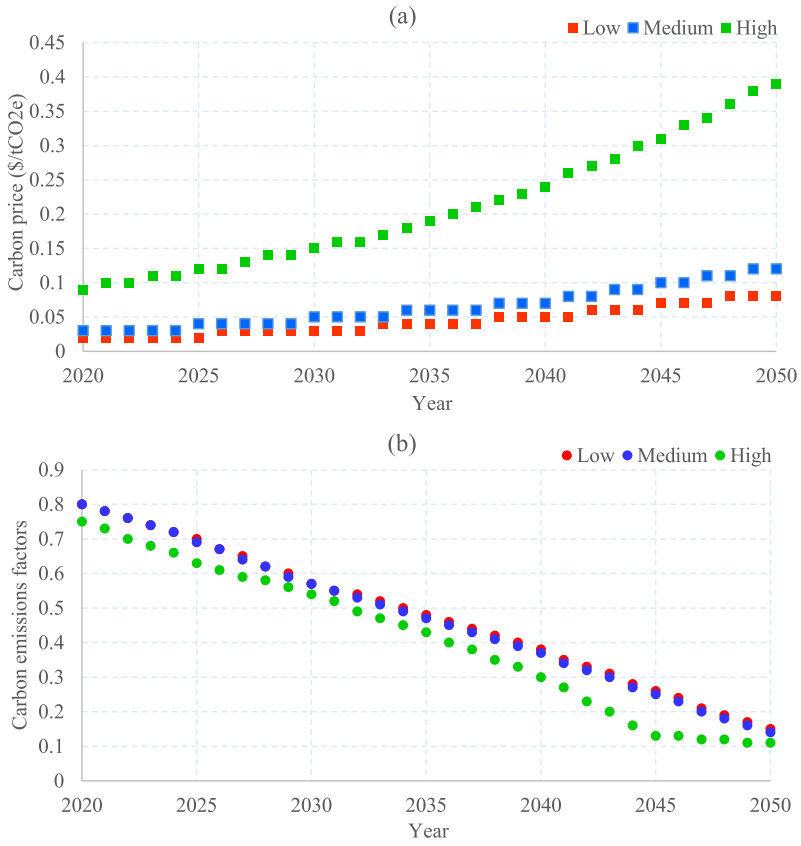

Fig. A1. Low, Medium, and High 2020 to 2050 projections for (a) CO_2 price, (b) CO_2 emissions factors relative to base year. NIST [50].

Appendix B

Table B1 displays the network cost estimation methods for piping and trenching from previous international studies.

Table B1
District heating and cooling network costs estimation methods for piping and trenching.

Study	Year	Country	Estimation Method	Currency	Network
Morvaj et al. [55]	2016	Switzerland	Fixed cost	€	DH
Persson et al. [56]	2011	Sweden	Formula	€	DH
Sommer et al. [57]	2020	Switzerland	Industry	€	DHC
Leurent et al. [58]	2018	France	Formula	€	DH†
Rieder et al. [59]	2014	Germany	Fixed cost	€	DH
Hirsch et al. [60]	2016	Poland	Formula	€	DH†
Togawa et al. [61]	2014	Japan	Formula	¥	DH
Dalla Rosa et al. [62]	2012	Canada	Industry	C$	DH
Chinese [63]	2008	Italy	Industry	€	DHC
Best et al. [12]	2020	USA	Industry	$	DHC
Dobersek et al. [64]	2009	Slovenia	Formula	€	DH
Nussbaumer et al. [49]	2016	Switzerland	Industry	€	DH
Li and Svendsen [65]	2013	Denmark	Industry	€	DH
Mertz et al. [10]	2016	France	Industry	€	DH
van der Heidge et al. [66]	2019	Belgium	Formula	€	DH
Marty et al. [67]	2018	France	Government	€	DH
Allen et al. [45]	2021	USA	Industry	$	DHC

†Large scale network for nuclear power plant heat distribution. Industry = price calculated using data sourced from commercial bodies, Formula = price calculated using equations and pipe dimensions, Government = price calculated based on government report, Fixed cost = static piping and trenching price per unit length (not based on pipe dimensions). DH = District Heating, DHC = District Heating & Cooling.

References

[1] Buffa S, Cozzini M, D'Antoni M, Baratieri M, Fedrizzi R. 5th generation district heating and cooling systems: a review of existing cases in Europe. Renew Sustain Energy Rev 2019;104:504–22. https://doi.org/10.1016/j.rser.2018.12.059.

[2] Lund H, et al. 4th Generation District Heating (4GDH): Integrating smart thermal grids into future sustainable energy systems. Energy 2014;68:1–11. https://doi.org/10.1016/j.energy.2014.02.089.

[3] Yuan S, Grabon M. Optimizing energy consumption of a water-loop variable-speed heat pump system. Appl Therm Eng 2011;31(5):894–901. https://doi.org/10.1016/j.applthermaleng.2010.11.012.

[4] Buonomano A, Calise F, Palombo A. Buildings dynamic simulation: Water loop heat pump systems analysis for European climates. Appl Energy 2012;91(1):222–34. https://doi.org/10.1016/j.apenergy.2011.09.031.

[5] Coccia G, D'Agaro P, Cortella G, Polonara F, Arteconi A. Demand side management analysis of a supermarket integrated HVAC, refrigeration and water loop heat pump system. Appl Therm Eng 2019;152:543–50. https://doi.org/10.1016/j.applthermaleng.2019.02.101.

[6] von Rhein J, Henze GP, Long N, Fu Y. Development of a topology analysis tool for fifth-generation district heating and cooling networks. Energy Convers Manag 2019;196:705–16. https://doi.org/10.1016/j.enconman.2019.05.066.

[7] Linn Laurberg, Jensen, Daniel Trier, Marcus; Brennenstuhl, Marco; Cozzini, Belen Ǵomez-Uribarri Serrano. D3 . 1 – analysis of network layouts in selected urban contexts. PlanEnergi, Technical report; 2017.

[8] Schluck T, Kräuchi P, Sulzer M. Non-linear thermal networks – How can a meshed network improve energy efficiency? 2015.

[9] Zarin Pass R, Wetter M, Piette MA. A thermodynamic analysis of a novel bidirectional district heating and cooling network. Energy 2018;144:20–30. https://doi.org/10.1016/j.energy.2017.11.122.

[10] Mertz T, Serra S, Henon A, Reneaume J-M. A MINLP optimization of the configuration and the design of a district heating network: Academic study cases. Energy 2016;117:450–64. https://doi.org/10.1016/j.energy.2016.07.106.

[11] Falke T, Krengel S, Meinerzhagen A-K, Schnettler A. Multi-objective optimization and simulation model for the design of distributed energy systems. Appl Energy 2016;184:1508–16. https://doi.org/10.1016/j.apenergy.2016.03.044.

[12] Best RE, Rezazadeh Kalehbasti P, Lepech MD. A novel approach to district heating and cooling network design based on life cycle cost optimization. Energy 2020;194:116837. https://doi.org/10.1016/j.energy.2019.116837.

[13] Lund H, et al. Perspectives on fourth and fifth generation district heating. Energy 2021;227:120520. https://doi.org/10.1016/j.energy.2021.120520.

[14] Gjoka K, Rismanchi B, Crawford RH. Fifth-generation district heating and cooling systems: a review of recent advancements and implementation barriers. Renew Sustain Energy Rev 2023;171:112997. https://doi.org/10.1016/j.rser.2022.112997.

[15] Wirtz M, Schreiber T, Müller D. Survey of 53 Fifth-Generation District Heating and Cooling (5GDHC) Networks in Germany. Energy Technol 2022;10(11):2200749. https://doi.org/10.1002/ente.202200749.

[16] Bilardo M, Sandrone F, Zanzottera G, Fabrizio E. Modelling a fifth-generation bidirectional low temperature district heating and cooling (5GDHC) network for nearly Zero Energy District (nZED). Energy Rep 2021;7:8390–405. https://doi.org/10.1016/j.egyr.2021.04.054.

[17] Chicherin S. Amount of heat available from a prosumer of a 5th generation district heating and cooling (5GDHC) system: case study of a data center. J Build Eng 2023;76:107138. https://doi.org/10.1016/j.jobe.2023.107138.

[18] Meibodi SS, Loveridge F. The future role of energy geostructures in fifth generation district heating and cooling networks. Energy 2022;240:122481. https://doi.org/10.1016/j.energy.2021.122481.

[19] Revesz A, et al. Developing novel 5th generation district energy networks. Energy 2020;201:117389. https://doi.org/10.1016/j.energy.2020.117389.

[20] Fröling M, Svanström M. Life cycle assessment of the district heat distribution system - Part 2: Network construction (11 pp). Int J Life Cycle Assess 2005;10(6):425–35. https://doi.org/10.1065/lca2004.12.195.

[21] Fröling M, Holmgren C, Svanström M. Life cycle assessment of the district heat distribution system. Int J Life Cycle Assess 2004;9(2):130–6. https://doi.org/10.1007/BF02978572.

[22] Persson C, Fröling M, Svanström M. Life cycle assessment of the district heat distribution system. Part 3: Use phase and overall discussion (10 pp). Int J Life Cycle Assess 2006;11(6):437–46. https://doi.org/10.1065/lca2005.08.225.

[23] Famiglietti J, et al. Environmental Life Cycle Assessment scenarios for a district heating network. An Italian case study. Energy Rep 2021;7:368–79. https://doi.org/10.1016/j.egyr.2021.08.094.

[24] Eriksson O, Finnveden G, Ekvall T, Björklund A. Life cycle assessment of fuels for district heating: a comparison of waste incineration, biomass- and natural gas combustion. Energy Policy 2007;35(2):1346–62. https://doi.org/10.1016/j.enpol.2006.04.005.

[25] Björnebo L, Spatari S, Gurian PL. A greenhouse gas abatement framework for investment in district heating. Appl Energy 2018;211:1095–105. https://doi.org/10.1016/j.apenergy.2017.12.003.

[26] Wirtz M, Kivilip L, Remmen P, Mueller D. 5th Generation District Heating: a novel design approach based on mathematical optimization, vol. 260. 2020. 10.1016/j.apenergy.2019.114158.

[27] Volkova A, Pakere I, Murauskaite L, Huang P, Lepiksaar K, Zhang X. 5th generation district heating and cooling (5GDHC) implementation potential in urban areas with existing district heating systems. Energy Rep 2022;8:10037–47. https://doi.org/10.1016/j.egyr.2022.07.162.

[28] Allen A, Henze G, Baker K, Pavlak G, Murphy M. An optimization framework for the network design of advanced district thermal energy systems. Energy Convers Manag 2022;266:115839. https://doi.org/10.1016/j.enconman.2022.115839.

[29] Doe. Commercial prototype building models. US Dep. Energy DOE; 2018.

[30] Modelica Association Project. Modelica language. [Online]. <https://www.modelica.org/modelicalanguage>.

[31] Franklin Associates. Cradle-To-Gate Life Cycle Inventory of Nine Plastic Resins and Four Polyurethane Precursors. American Chemistry Council. Accessed: Nov. 11, 2023. [Online]. <https://www.americanchemistry.com/better-policy-regulation/plastics/resources/cradle-to-gate-life-cycle-inventory-of-nine-plastic-resins-and-four-polyurethane-precursors>.

[32] REHAU. Engineering progress enhancing lives: heat network solutions. REHAU; 2020.

[33] Chilana L, Bhatt AH, Najafi M, Sattler M. Comparison of carbon footprints of steel versus concrete pipelines for water transmission. J Air Waste Manag Assoc 2016;66(5):518–27. https://doi.org/10.1080/10962247.2016.1154487.

[34] IEEP. Environmentally harmful subsidies: identification and assessment, annex 5: subsidy level indicators for the case studies. European Commission, DG Environment.

[35] "2012 ASHRAE Handbook - Heating, Ventilating, and Air-Conditioning Systems and Equipment (SI Edition)." Accessed: Nov. 11, 2023. [Online]. <https://app.knovel.com/kn/resources/kpASHRAEA2/toc>.

[36] Du F, Woods GJ, Kang D, Lansey KE, Arnold RG. Life cycle analysis for water and wastewater pipe materials. J Environ Eng 2013;139(5):703–11. https://doi.org/10.1061/(ASCE)EE.1943-7870.0000638.

[37] Jakhrani AQ, Rigit ARH, Othman A-K, Samo SR, Kamboh SA. Estimation of carbon footprints from diesel generator emissions. In: 2012 International Conference on Green and Ubiquitous Technology, Jul. 2012, pp. 78–81. 10.1109/GUT.2012.6344193.

[38] Venkatesh G, Hammervold J, Brattebø H. Combined MFA-LCA for analysis of wastewater pipeline networks: case study of Oslo, Norway. J Ind Ecol 2009;13:532–50. https://doi.org/10.1111/j.1530-9290.2009.00143.x.

[39] Wahlroos M, Pärssinen M, Rinne S, Syri S, Manner J. Future views on waste heat utilization – case of data centers in Northern Europe. Renew Sustain Energy Rev 2018;82:1749–64. https://doi.org/10.1016/j.rser.2017.10.058.

[40] Davies GF, Maidment GG, Tozer RM. Using data centres for combined heating and cooling: an investigation for London. Appl Therm Eng 2016;94:296–304. https://doi.org/10.1016/j.applthermaleng.2015.09.111.

[41] Attalla M, Maghrabie HM. Investigation of effectiveness and pumping power of plate heat exchanger with rough surface. Chem Eng Sci 2020;211:115277. https://doi.org/10.1016/j.ces.2019.115277.

[42] D. Sickinger, D. Martinez, and B. Bolz, "Energy Performance Evaluation of Aquila's Aquarius Fixed Cold Plate Cooling System at NREL's High Performance Computing Center," 2019, 10.2172/1497991.

[43] Sickinger DE, Van Geet OD, Belmont SA, Carter T, Martinez D. Thermosyphon Cooler Hybrid System for Water Savings in an Energy-Efficient HPC Data Center: Results from 24 Months and the Impact on Water Usage Effectiveness. National Renewable Energy Lab Sep. 2018. https://doi.org/10.2172/1471661. NREL), Golden, CO (United States), NREL/TP-2C00-72196.

[44] Murphy MD. M-D-Murphy/Data-Centre-Waste-Heat. Feb. 14, 2024. Accessed: Feb. 14, 2024. [Online]. <https://github.com/M-D-Murphy/Data-Centre-Waste-Heat>.

[45] Allen A, Henze G, Baker K, Pavlak G, Murphy M. Evaluation of topology optimization to achieve energy savings at the urban district level: preprint. National Renewable Energy Lab. (NREL), Golden, CO (United States), NREL/CP-5500-77625; Feb. 2021. Accessed: Nov. 11, 2023. [Online]. <https://www.osti.gov/biblio/1769805>.

[46] Fleschutz M, Bohlayer M, Braun M, Murphy MD. Demand response analysis framework (DRAF): an open-source multi-objective decision support tool for decarbonizing local multi-energy systems. Sustainability 2022;14(13):8025. https://doi.org/10.3390/su14138025.

[47] Phan QA, Scully T, Breen M, Murphy MD. Facilitating high levels of wind penetration in a smart grid through the optimal utilization of battery storage in microgrids: an analysis of the trade-offs between economic performance and wind generation facilitation. Energy Convers Manag 2020;206:112354. https://doi.org/10.1016/j.enconman.2019.112354.

[48] Breen M, Murphy MD, Upton J. Development of a dairy multi-objective optimization (DAIRYMOO) method for economic and environmental optimization of dairy farms. Appl Energy 2019;242:1697–711. https://doi.org/10.1016/j.apenergy.2019.03.059.

[49] Nussbaumer T, Thalmann S. Influence of system design on heat distribution costs in district heating. Energy 2016;101:496–505. https://doi.org/10.1016/j.energy.2016.02.062.

[50] Lavappa P, Kneifel JD. Energy price indices and discount factors for life-cycle cost analysis - 2020 annual supplement to NIST handbook 135," *NIST*, Apr. 2020, Accessed: Nov. 11, 2023. [Online]. <https://www.nist.gov/publications/energy-price-indices-and-discount-factors-life-cycle-cost-analysis-2020-annual>.

[51] World Bank, "State and Trends of Carbon Pricing 2020,"; 2020. Accessed: Nov. 11, 2023. [Online]. <http://hdl.handle.net/10986/33809>.

[52] "Emissions Factors 2022 – Data product," IEA. Accessed: Nov. 11, 2023. [Online]. <https://www.iea.org/data-and-statistics/data-product/emissions-factors-2022>.

[53] Rennert K, et al. Comprehensive evidence implies a higher social cost of CO2. Art. no. 7933 Nature 2022;610(7933). https://doi.org/10.1038/s41586-022-05224-9.

[54] Kozubal EJ. Innovation incubator: liquidcool solutions technical evaluation. laboratory study and demonstration results of a directed-flow, liquid submerged server for high-efficiency data centers. National Renewable Energy Lab. (NREL), Golden, CO (United States), NREL/TP-5500-70459; 2017. 10.2172/1413900.

[55] Morvaj B, Evins R, Carmeliet J. Optimising urban energy systems: Simultaneous system sizing, operation and district heating network layout. Energy 2016;116:619–36. https://doi.org/10.1016/j.energy.2016.09.139.
[56] Persson U, Werner S. Heat distribution and the future competitiveness of district heating. Appl Energy 2011;88(3):568–76. https://doi.org/10.1016/j.apenergy.2010.09.020.
[57] Sommer T, Sulzer M, Wetter M, Sotnikov A, Mennel S, Stettler C. The reservoir network: a new network topology for district heating and cooling. Energy 2020;199:117418. https://doi.org/10.1016/j.energy.2020.117418.
[58] Leurent M, Da Costa P, Jasserand F, Rämä M, Persson U. Cost and climate savings through nuclear district heating in a French urban area. Energy Policy 2018;115:616–30. https://doi.org/10.1016/j.enpol.2018.01.043.
[59] Rieder A, Christidis A, Tsatsaronis G. Multi criteria dynamic design optimization of a small scale distributed energy system. Energy 2014;74:230–9. https://doi.org/10.1016/j.energy.2014.06.007.
[60] Hirsch P, Duzinkiewicz K, Grochowski M, Piotrowski R. Two-phase optimizing approach to design assessments of long distance heat transportation for CHP systems. Appl Energy 2016;182:164–76. https://doi.org/10.1016/j.apenergy.2016.08.107.
[61] Togawa T, Fujita T, Dong L, Fujii M, Ooba M. Feasibility assessment of the use of power plant-sourced waste heat for plant factory heating considering spatial configuration. J Clean Prod 2014;81:60–9. https://doi.org/10.1016/j.jclepro.2014.06.010.
[62] Dalla Rosa A, Boulter R, Church K, Svendsen S. District heating (DH) network design and operation toward a system-wide methodology for optimizing renewable energy solutions (SMORES) in Canada: a case study. Energy 2012;45(1):960–74. https://doi.org/10.1016/j.energy.2012.06.062.
[63] Chinese D. Optimal size and layout planning for district heating and cooling networks with distributed generation options. Int J Energy Sect Manag 2008;2:385–419. https://doi.org/10.1108/17506220810892946.
[64] Dobersek D, Goricanec D. Optimisation of tree path pipe network with nonlinear optimisation method. Appl Therm Eng 2009;29(8):1584–91. https://doi.org/10.1016/j.applthermaleng.2008.07.017.
[65] Li H, Svendsen S. District Heating Network Design and Configuration Optimization with Genetic Algorithm. J Sustain Dev Energy Water Environ Syst 2013;1(4):291–303. https://doi.org/10.13044/j.sdewes..2013.01.22.
[66] van der Heijde B, Vandermeulen A, Salenbien R, Helsen L. Integrated optimal design and control of fourth generation district heating networks with thermal energy storage. Art. no. 14 Energies 2019;12(14). https://doi.org/10.3390/en12142766.
[67] Marty F, Serra S, Sochard S, Reneaume J-M. Simultaneous optimization of the district heating network topology and the Organic Rankine Cycle sizing of a geothermal plant. Energy 2018;159:1060–74. https://doi.org/10.1016/j.energy.2018.05.110.